Indian Journal of Chemistry
Vol. 63, December 2024, pp. 1271-1293
DOI: 10.56042/ijc.v63i12.14198

Multifaceted analysis of intermolecular interactions in α-terpineol-halobenzenes binary mixtures: Insights from thermophysical, acoustical, and spectral techniques, supported by quantum computational approaches

Paras Patel*[a] & Sangita Sharma[b]

[a] Department of Chemistry, Indus Institute of Sciences, Humanities & Liberal Studies (IISHLS), Indus University, Ahmedabad 382 115, Gujarat, India

[b] Department of Chemistry, Hemchandracharya North Gujarat University, Patan 384 265, Gujarat, India

E-mail: paras12patel@yahoo.com, paraspatel.gd@indusuni.ac.in

Received 25 October 2024; accepted (revised) 27 November 2024

This study examines the thermophysical, acoustical, and spectral properties of binary mixtures of α-terpineol with fluorobenzene, chlorobenzene, and bromobenzene under standard atmospheric pressure at 303.15 K, 308.15 K and 313.15 K. Molar volume (V_m), excess molar volume (V_m^E), partial molar volume ($\bar{V}_{m,i}^o$), excess partial molar volume ($\bar{V}_{m,i}^{o,E}$), apparent molar volume ($V_{m,\Phi,i}$), deviation in speed of sound (Δu), isentropic compressibility (κ_s), deviation in isentropic compressibility ($\Delta\kappa_s$), acoustical impedance (z), deviation in acoustical impedances (Δz), intermolecular free length (L_f), partial molar isentropic compression ($\bar{K}_{s,m,i}^o$), excess partial molar isentropic compression ($\bar{K}_{s,m,i}^{o,E}$), and apparent molar isentropic compression ($K_{s,m,\Phi,i}$) have been measured. Parameters such as infinite dilution apparent molar volume ($V_{m,\Phi,1}^o$), infinite dilution apparent molar isentropic compression ($K_{s,m,\Phi,1}^o$) have also been determined. The Redlich-Rosenberg-Mayer equation for empirical coefficients and applied theoretical models to analyze speed of sound and deviation properties have been used. FT-IR spectral analysis has been performed on binary mixtures at 298.15 K, while computational investigations include gas phase optimization, Mulliken charges, vibrational frequencies, NCI, ELF, LOL, and NBO analyses using DFT. These studies elucidate intermolecular interactions, their strengths, and variations with temperature and halobenzene concentration.

Keywords: Binary mixtures, Density, Speed of sound, FT-IR, DFT

α-Terpineol, a monoterpene alcohol naturally found in essential oils, has captivated researchers due to its versatile applications in pharmaceutical and chemical fields. Its pharmacological properties, encompassing antimicrobial, anti-inflammatory, and analgesic effects, position it as a promising compound for pharmaceutical formulations and topical treatments[1,2]. Additionally, in the realm of chemical synthesis, α-terpineol serves as a crucial precursor for the production of fragrances, flavors, and various fine chemicals, contributing significantly to industrial processes[3,4].

Exploring the intermolecular interactions in binary mixtures of α-terpineol with halobenzenes is pivotal, particularly concerning the extraction of α-terpineol from plant extracts. Extraction procedures often rely on solvent systems, where the choice of solvent mixture is critical for achieving desired solubility and selective extraction of α-terpineol. A nuanced understanding of intermolecular interactions within these binary systems aids in refining extraction processes, enhancing the efficiency of α-terpineol recovery, and elevating the purity of the final product[5,6].

Moreover, an in-depth investigation into intermolecular interactions in α-terpineol-halobenzenes binary mixtures holds significance in both industrial production and analytical characterization of these compounds. These interactions exert influence across various industrial processes, spanning from the design of extraction and purification protocols to the optimization of reaction conditions[7,8]. Unravelling the behavior of these mixtures provides valuable insights into solvent-solute interactions, thereby facilitating the selection of optimal solvents and process parameters for large-scale production.

From an analytical standpoint, the study of α-terpineol frequently involves chromatographic techniques, wherein intermolecular interactions play a pivotal role in successful compound analysis.

Chromatographic separation and identification hinge upon the interactions between analyte molecules and stationary and mobile phases. A thorough comprehension of intermolecular forces within binary mixtures aids in tailoring chromatographic conditions to achieve optimal separation and detection of α-terpineol[9-11].

Intermolecular interactions, spanning dipole-dipole, dipole-induced dipole, and hydrogen bonding forces, profoundly influence the physicochemical behavior of molecules. These interactions, dictated by the nature and arrangement of functional groups, provide invaluable insights into molecular properties and reactivity.

In this study, we aim to delve into the behavior of α-terpineol within diverse solvent environments by examining its binary mixtures with halobenzenes. Halobenzenes, like fluorobenzene, chlorobenzene, and bromobenzene used here, serve as the second component in these binary mixtures, offering a platform to explore the effects of halogen substitution in benzene on intermolecular interactions. Through systematic exploration of binary mixtures of α-terpineol with halobenzenes at varying compositions and temperatures, we aspire to illuminate the intricate relationship between molecular structure and the strength and nature of intermolecular interactions.

This study endeavours to investigate intermolecular interactions in binary mixtures of α-terpineol with halobenzenes, incorporating an array of techniques encompassing thermophysical, acoustical, spectral, and computational aspects. A comprehensive analysis of these interactions, coupled with the correlation of experimental and computational findings, promises to furnish invaluable insights into the behavior of these mixtures. Ultimately, the outcomes of this study are poised to advance our fundamental understanding of intermolecular interactions and offer practical guidance for extraction, production, and analytical characterization of α-terpineol in diverse industrial and pharmaceutical applications.

Experimental Section

Materials and Chemicals

The chemicals utilized in this study were sourced from reputable suppliers and were of analytical reagent (AR) grade. Prior to their incorporation into experimental procedures, the chemicals underwent purification processes according to established protocols[12,13]. Table S1 of supplementary data presents a comprehensive overview of the chemical suppliers, purification techniques employed, CAS numbers, initial purities, purities post-purification, and the methodology utilized for purity assessment. To ensure the fidelity of our experimental findings, a comparative analysis between the measured density and speed of sound values and the corresponding literature values at the designated temperatures has been conductedand detailsare given in Table S2 of supplementary data. The data in Table S2 underscore a close concordance between our experimental results and literature references.

Apparatus and Experimental Procedures

Sample Preparation

Each binary mixture was meticulously prepared by precisely blending the two components using an electronic balance (Reptech-RA-2012) with a weight accuracy of ±0.0001 g. To mitigate solvent evaporation, all mixtures were prepared in specialized ground glass airtight ampoules. Furthermore, the ampoules were shielded from light exposure to minimize potential photolytic effects, ensuring the stability and integrity of the binary mixtures throughout the experimental regimen.

Density (ρ) and Speed of Sound (u) Measurement

The determination of density and speed of sound values for both pure components and their binary mixtures was executed using an automated density and speed of sound measuring instrument (Model: DSA 5000M, Anton Paar, India). The instrument boasts high precision, with a measuring accuracy of ±0.000005 $g \cdot cm^{-1}$ for density and ±0.1 $m \cdot s^{-1}$ for speed of sound. Temperature control was maintained during measurements *via* the instrument's integrated temperature control system, ensuring an accuracy of ±0.001°C (0.002°F). Preceding measurements, the instrument underwent calibration using highly pure deionized water provided by the manufacturer.

FT-IR Spectra Measurement

FT-IR spectra of both pure components and their binary mixtures were measured using an alpha-FT-IR spectrometer (Bruker, Germany), featuring a resolution of 2 cm^{-1} and a scan rate of 4 scans. Measurements were conducted at a temperature of 298.15K, with spectra recorded at varying composition ratios of 4:1, 1:1, and 1:4 (v/v%). To ensure data accuracy, FT-IR spectra underwent correction to account for potential water vapor and CO_2 interference, facilitating a precise analysis of the samples.

Quantum Computational Calculations

Quantum computational calculations, encompassing geometrical optimization, vibrational analysis, and energy calculations including NBO analysis, were conducted for both pure components and their binary mixtures in the gas phase. These calculations employed a hybrid function of the Density Functional Theory (DFT) method, specifically Beck's three-parameter exchange functional B3, coupled with the Lee-Yang-Par (LYP) corrected correlation function with 6-31+G(d,p) basis set was employed[14-30]. The validity of optimized structures was confirmed by the absence of imaginary frequencies in vibrational calculations. Gaussian 16[31] facilitated all quantum computational calculations and results were visualized using Gauss View 6[32]. The wave function analyses such as Non-Covalent Interactions (NCI) analyses, Electron Localization Function (ELF), and Localized Orbital Locator (LOL) were carried out by Multiwfn 3.8(dev) program[33]. The Non-Covalent Interactions (NCI) plots were extracted by Visual Molecular Dynamics (VMD) 1.9.4 program[34] based on the outputs of Multiwfn analyser.

Mathematical Framework and Property Analysis

In this section, the mathematical models and relations essential for analyzing and interpreting experimental data concerning binary mixtures have been mentioned. These mathematical tools provide important insights into the behavior and properties of the studied systems.

Molar Volume ($\mathbf{V_m}$)

The molar volume (V_m) serves as a fundamental property derived from density measurements. It characterizes the spatial arrangement of molecules within a system and is governed by various factors including intermolecular interactions, molecular size, and shape. For pure components, the molar volume (V_m) can be calculated using the relationship:

$$V_i(cm^3.mol^{-1}) = \frac{M_i}{\rho_i} \quad \ldots (1)$$

where M_i is the molar mass and ρ_i is the density of the i^{th}component. For binary mixtures, the molar volume (V_m) is determined by:

$$V_m(cm^3.mol^{-1}) = \frac{M_1x_1+M_2x_2}{\rho_m} \quad \ldots (2)$$

Here, $x_1$and x_2 represent the mole fractions of component 1 and component 2, respectively.

Excess Molar Volume ($\mathbf{V_m^E}$)

The excess molar volume (V_m^E) quantifies the deviation from ideal behavior in a solution, reflecting the presence and strength of intermolecular interactions. It can be calculated by:

$$V_m^E(cm^3.mol^{-1}) = V_m - V_1x_1 - V_2x_2 \quad \ldots (3)$$

Alternatively, a generalized form of excess molar volume can be expressed as:

$$V_m^E(cm^3.mol^{-1}) = \left(\frac{x_1M_1 + x_2M_2}{\rho_m}\right) - \left(\frac{x_1M_1}{\rho_1}\right) - \left(\frac{x_2M_2}{\rho_2}\right) \quad \ldots (4)$$

The sign and magnitude of V_m reveal the nature of intermolecular interactions, with positive values indicating repulsive forces and negative values indicating attractive forces.

Partial Molar Volume($\mathbf{\bar{V}^o_{m,i}}$) and Excess Partial Molar Volume ($\mathbf{\bar{V}^{o,E}_{m,i}}$)

Partial molar volume ($\bar{V}^o_{m,i}$) characterizes the volume contribution of each component in a mixture, while excess partial molar volume ($\bar{V}^{o,E}_{m,i}$) indicates deviations from ideal mixing. The partial molar volume ($\bar{V}^o_{m,i}$)and excess partial molar volume ($\bar{V}^{o,E}_{m,i}$) of the components in their binary mixtures were calculated using the following relations[35]:

For component 1:

$$\bar{V}^o_{m,1} = V_m^E + V^*_{m,1} + x_2\left(\frac{\partial V_m^E}{\partial x_1}\right)_{T,P} \quad \ldots (5)$$

For component 2:

$$\bar{V}^o_{m,2} = V_m^E + V^*_{m,2} - x_1\left(\frac{\partial V_m^E}{\partial x_1}\right)_{T,P} \quad \ldots (6)$$

Here, V_m^E signifies the excess molar volume of the mixture, while $V^*_{m,1}$and $V^*_{m,2}$ represent the molar volumes of component 1 and component 2, respectively. $\bar{V}^o_{m,1}$and $\bar{V}^o_{m,2}$represent the partial molar volumes of component 1 and component 2, respectively.

By evaluating the derivative $\left(\frac{\partial V_m^E}{\partial x_1}\right)_{T,P}$, we can derive the expressions for the partial molar volumes:
For component 1:

$$\bar{V}^o_{m,1} = V^*_{m,1} + x_2^2\sum_{i=0}^{n} A_i(1-2x_1)^i - 2x_1x_2^2\sum_{i=1}^{n} A_i(1-2x_1)^{i-1} \quad \ldots (7)$$

For component 2:

$$\bar{V}^{o}_{m,2} = V^{*}_{m,2} + x_1^2 \sum_{i=0}^{n} A_i (1-2x_1)^i + 2x_1^2 x_2 \sum_{i=1}^{n} A_i (1-2x_1)^{i-1} \quad \ldots (8)$$

Next, the excess partial molar volumes are determined using the following relations:

For component 1:

$$\bar{V}^{o,E}_{m,1}(cm^3.mol^{-1}) = \bar{V}^{o}_{m,1} - V^{*}_{m,1} \quad \ldots (9)$$

For component 2:

$$\bar{V}^{o,E}_{m,2}(cm^3.mol^{-1}) = \bar{V}^{o}_{m,2} - V^{*}_{m,2} \quad \ldots (10)$$

where, $\bar{V}^{o}_{m,1}$ and $\bar{V}^{o}_{m,2}$ represent the partial molar volumes of component 1 and component 2, respectively.

These equations allow for the detailed calculation of partial molar volumes and excess partial molar volumes, providing valuable insights into the volume contributions of each component and the deviations from ideal mixing behavior. Subsequently, the obtained results will be thoroughly discussed, shedding light on the intricate intermolecular interactions and their implications on the properties of the analyzed binary mixtures[35].

Apparent Molar Volume $\left(\mathbf{V_{m,\Phi,i}}\right)$

To calculate the apparent molar volume across all binary mixtures, two distinct methodologies were employed, outlined as follows:

Method 1[36]:

The apparent molar volume, $V_{m,\phi,i}$, was computed using the subsequent expression:

$$V_{m,\phi,i}(cm^3.mol^{-1}) = \frac{M}{\rho} - \frac{(\rho-\rho_o)}{m\rho\rho_o} \quad \ldots (11)$$

Here, M denotes the molar mass of solute molecules, m represents solute molality, ρ signifies the solution density, and ρ_o stands for the density of solute molecules.

Method 2:

The apparent molar volume, $V'_{m,\phi,i}$, was calculated using the following relations:

$$V'_{m,\phi,1}(cm^3.mol^{-1}) = \left(\frac{V_m - (1-x_1)\bar{V}^{o}_{m,2}}{x_1}\right) \quad \ldots (12)$$

$$V'_{m,\phi,2}(cm^3.mol^{-1}) = \left(\frac{V_m - x_1\bar{V}^{o}_{m,1}}{(1-x_1)}\right) \quad \ldots (13)$$

Upon substituting the equation for V^{E}_{m} into the above formulations, we derive:

$$V'_{m,\phi,1}(cm^3.mol^{-1}) = \bar{V}^{o}_{m,1} + \left(\frac{V^{E}_{m}}{x_1}\right) \quad \ldots (14)$$

$$V'_{m,\phi,2}(cm^3.mol^{-1}) = \bar{V}^{o}_{m,2} + \left(\frac{V^{E}_{m}}{x_2}\right) \quad \ldots (15)$$

In these equations, $V'_{m,\phi,1}$ and $V'_{m,\phi,2}$ signify the apparent molar volumes of component 1 and component 2, respectively.

The determination of apparent molar volume offers critical insights into volume alterations upon solute addition to the solvent. It aids in comprehending solute-solvent interactions and their influence on the overall volume dynamics within binary mixtures. By employing these methodologies, we can discern volume fluctuations concerning composition and unravel intricate molecular interactions and structural transformations within the mixtures.

Infinite Dilution Apparent Molar Volume $\left(\mathbf{V^{o}_{m,\Phi,1}}\right)$ and Empirical Parameters $\mathbf{S_v}$, $\mathbf{B_v}$ using the Redlich-Rosenberg-Mayer Equation

The determination of the infinite dilution apparent molar volume, $V^{o}_{m,\Phi,1}$, across all binary mixtures was calculated through the utilization of the Redlich-Rosenberg-Mayer equation[36]:

$$V_{m,\phi,1} = V^{o}_{m,\phi,1} + S_v m^{\frac{1}{2}} + B_v m \quad \ldots (16)$$

Here, S_v and B_v represent empirical parameters that encapsulate the impact of solute concentration (m) on the apparent molar volume of component 1 within the mixture. The Redlich-Rosenberg-Mayer equation furnishes a quantitative framework for elucidating the concentration-dependent behavior of the apparent molar volume, enabling the determination of $V^{o}_{m,\Phi,1}$ alongside the derivation of S_v and B_v. These empirical parameters serve as invaluable indicators of solute-solvent interactions and the accompanying structural alterations within the binary mixtures.

Limiting Apparent Molar Expansibility $\left(\mathbf{E^{o}_{\Phi}}\right)$

The calculation of limiting apparent molar expansibility (E^{o}_{Φ}) across all binary mixtures was undertaken employing the following relationships[36]:

The temperature variation of $V^{o}_{m,\phi,i}$ can be delineated *via* the equation:

$$V^{o}_{m,\phi,i} = A + BT + CT^2 \quad \ldots (17)$$

Where in, A, B, and C denote temperature-dependent constants of $V^{o}_{m,\phi,i}$.

The determination of (E^{o}_{Φ}) is attained by differentiating the above equation with respect to temperature (T):

$$E^{o}_{\phi} = \left(\frac{\partial V^{o}_{\phi}}{\partial T}\right) = B + 2CT \quad \ldots (18)$$

These formulations facilitate the exploration of the temperature-responsive characteristics of the apparent molar volume, enabling the extraction of E_{Φ}^{o}. Furthermore, the determination of A, B, and Ccontributes to the delineation of the temperature-dependent attributes of $V_{m,\phi,i}^{o}$, thereby enhancing our comprehension of the thermodynamic traits inherent in the examined mixtures. The subsequent sections will delve into the discussion and analysis of these properties and their temperature dependencies, unraveling the underlying molecular interactions and the repercussions of temperature fluctuations on the behavior of the binary mixtures.

Deviation in Speed of Sound ($\Delta\mathbf{u}$)

The calculation of deviations in the speed of sound (Δu) is conducted utilizing the subsequent formulations:

$$\Delta u\ (m \cdot s^{-1}) = u_{exp} - (x_1u_1 + x_2u_2) \quad \ldots (19)$$

$$\Delta u\ (m \cdot s^{-1}) = u_{exp} - (x_1u_1 + x_2u_2 + x_3u_3) \quad \ldots (20)$$

Herein, u_{exp} denotes the speed of sound of the mixture, while x_1 and x_2 signify the mole fractions, and u_1 and u_2 represent the speeds of sound of pure components 1 and 2, respectively. The analysis of deviations in speed of sound offers valuable insights into the alterations in sound propagation within binary mixtures. By juxtaposing the experimental speed of sound against the anticipated values derived from the individual components, the deviation (Δu) is ascertained. Such scrutiny aids in elucidating the impact of composition on the acoustic characteristics exhibited by the mixture.

Isentropic Compressibility ($\mathbf{k_s}$), Deviation in Isentropic Compressibility ($\Delta\mathbf{k_s}$), Acoustical Impedance ($\mathbf{z}$), Deviation in Acoustical Impedance ($\Delta\mathbf{z}$), and Intermolecular Free Length ($\mathbf{L_f}$)

The calculation of these properties is facilitated through the utilization of the subsequent equations[37]:

$$k_s(T\ Pa^{-1}) = \frac{1}{u_i^2\rho_i} \quad \ldots (21)$$

$$Z\ (g \cdot m^{-2} \cdot s^{-1}) = u_i\rho_i \quad \ldots (22)$$

$$L_f = Kk_s^{\frac{1}{2}} \quad \ldots (23)$$

$$\Delta k_s = k_{s_{exp}} - \left(x_1k_{s_1} + x_2k_{s_2}\right) \quad \ldots (24)$$

$$\Delta z = z_{exp} - (x_1z_1 + x_2z_2) \quad \ldots (25)$$

Herein, x_1, and $x_2$denote the mole fractions, ϕ_1 and ϕ_2 represent the volume fractions, $k_{s_1}$and k_{s_2} denote the isentropic compressibilities, z_1 and z_2 represent the acoustical impedances of components 1 and 2. $k_{s_{exp}}$ and z_{exp} represent the isentropic compressibility and acoustical impedance of the binary mixture, respectively. u_i and ρ_i represent the speed of sound and density of the i^{th} component, and K is the temperature-dependent Jacobson constant. These properties furnish insightful details concerning the compressibility and acoustic behavior of the mixture. Deviations in isentropic compressibility (Δk_s) and acoustical impedance (Δz) delineate the impact of composition on the compressibility and sound propagation characteristics. The intermolecular free length (L_f) signifies the average distance between molecules in the mixture, thereby reflecting the molecular interactions and arrangement.

Partial Molar Isentropic Compressibility ($\mathbf{K_{s,m,\Phi,i}}$) and Excess Partial Molar Isentropic Compressibility ($\mathbf{\overline{K}^{o,E}_{s,m,i}}$)

The partial molar isentropic compressibility ($K_{s,m,\Phi,i}$) and excess partial molar isentropic compressibility ($\overline{K}^{o,E}_{s,m,i}$) are determined utilizing the following equations[37]:

$$\overline{K}^{o}_{s,m,1} = K^{E}_{s,m} + K^{*}_{s,m,1} + x_2\left(\frac{\partial K^{E}_{s,m}}{\partial x_1}\right)_{T,P} \quad \ldots (26)$$

$$\overline{K}^{o}_{s,m,2} = K^{E}_{s,m} + K^{*}_{s,m,2} - x_1\left(\frac{\partial K^{E}_{s,m}}{\partial x_1}\right)_{T,P} \quad \ldots (27)$$

By differentiating $\left(\frac{\partial K^{E}_{s,m}}{\partial x_1}\right)_{T,P}$, the following relationships are derived:

$$\overline{K}^{o}_{s,m,1} = K^{*}_{s,m,1} + x_2^2\sum_{i=0}^{n} A_i(1-2x_1)^i - 2x_1x_2^2\sum_{i=1}^{n} A_i(1-2x_1)^{i-1} \quad \ldots (28)$$

$$\overline{K}^{o}_{s,m,2} = K^{*}_{s,m,2} + x_1^2\sum_{i=0}^{n} A_i(1-2x_1)^i + 2x_1^2x_2\sum_{i=1}^{n} A_i(1-2x_1)^{i-1} \quad \ldots (29)$$

Furthermore, the excess partial molar isentropic compressibility is expressed as:

$$\overline{K}^{o,E}_{s,m,1}((TPa)^{-1} \cdot m^3 \cdot\ mol^{-1}) = \overline{K}^{o}_{s,m,1} - K^{*}_{s,m,1} \quad \ldots (30)$$

$$\overline{K}^{o,E}_{s,m,2}((TPa)^{-1} \cdot m^3 \cdot\ mol^{-1}) = \overline{K}^{o}_{s,m,2} - K^{*}_{s,m,2} \quad \ldots (31)$$

Here, $K^{E}_{s,m}$ denotes the excess molar isentropic compressibility of the mixture, $K^{*}_{s,m,1}$, $K^{*}_{s,m,2}$ are the molar isentropic compressibilities, and $\overline{K}^{o}_{s,m,1}$, $\overline{K}^{o}_{s,m,2}$ represent the partial molar isentropic compressibilities of components 1 and 2, respectively. These properties

aid in understanding the contribution of individual components to the compressibility behavior of the mixture, encompassing the excess effects due to component interactions.

Apparent Molar Isentropic Compressibility $(\mathbf{K_{s,m,\phi,i}})$ and Redlich-Rosenberg-Mayer Equation

The calculation of the apparent molar isentropic compressibility $(K_{s,m,\phi,i})$is carried out through two methods[36,37]:

Method 1:

$$K_{s,m,\phi,i} = \frac{K_s M}{\rho} - \frac{1000(K_{s_o}\rho - K_s\rho_0)}{m\rho\rho_0} \quad \ldots (32)$$

Method 2:

$$K'_{s,m,\phi,1} = \bar{K}^0_{s,m,1} + \left(\frac{K^E_{s,m}}{x_1}\right) \quad \ldots (33)$$

$$K'_{s,m,\phi,2} = \bar{K}^0_{s,m,2} + \left(\frac{K^E_{s,m}}{x_2}\right) \quad \ldots (34)$$

Here, $K'_{s,m,\phi,1}$ and $K'_{s,m,\phi,2}$ represent the apparent molar isentropic compressibility of components 1 and 2, respectively. K_s, K_{s_o}, ρ, and $\rho_0$represent the isentropic compressibility of the mixture, isentropic compressibility of the solvent, density of the mixture, and density of the solvent, respectively.

Limiting Apparent Molar Isentropic Compressibility $(\mathbf{K^0_{s.m.\phi,i}})$ and The Redlich-Rosenberg-Mayer Equation

The calculation of the limiting apparent molar isentropic compressibility $(K^0_{s.m.\phi,i})$ is performed using the Redlich-Rosenberg-Mayer equation[36,37]:

$$K_{s,m,\phi,i}\ ((TPa)^{-1}\cdot m^3\cdot mol^{-1}) = K^0_{s.m.\phi,i} + S_k m^{\frac{1}{2}} + B_k m \quad \ldots (35)$$

Here, $K^0_{s.m.\phi,i}$ represents the limiting apparent molar isentropic compressibility of the i^{th} component, while S_k and B_k are empirical parameters. These computations offer insights into the compressibility behavior of components in mixtures, allowing for the assessment of their interactions and deviations from ideal behavior.

Theoretical Speed of Sound Relations

I. Junjie Equation[38]

The Junjie equation offers a theoretical framework for determining the speed of sound in binary mixtures, expressed as:

$$u_{junji} = \left\{\left(\frac{x_1M_1}{\rho_1}\right) + \left(\frac{x_2M_2}{\rho_2}\right)\right\} / \left\{(x_1M_1 + x_2M_2)^{\frac{1}{2}}\left[\left(\frac{x_1V_1}{\rho_1u_1^2}\right) + \left(\frac{x_2V_2}{\rho_2u_2^2}\right)^{1/2}\right]\right\} \quad \ldots (36)$$

Here, x_i, M_i, ρ_i and $u_i$denote the mole fraction, molar mass, density, and speed of sound of pure component 1 and 2, respectively.

II. Nomoto Equation[39]

The Nomoto equation presents an alternative theoretical approach for the speed of sound calculation in binary mixtures, given by:

$$u_{nom} = \left\{\frac{x_1R_1 + x_2R_2}{x_1V_1 + x_2V_2}\right\}^3 \quad \ldots (37)$$

where,V_i represents the molar volume of pure component 1 and 2, and R_i is Wada's constant obtained by using the following relation.

$$R_i = u_i^{1/3}V_i \quad \ldots (38)$$

Here, u_i represents the speed of sound of the i^{th} component.

III. Ideal Mixture Relation[40]

The ideal mixture relation simplifies the theoretical estimation of speed of sound and is given by:

$$u_{imr} = [1/(x_1M_1 + x_2M_2)^{1/2}]\left\{1/\left[\left(\frac{x_1}{M_1u_1^2}\right) + \left(\frac{x_2}{M_2u_2^2}\right)\right]^{1/2}\right\} \quad \ldots (39)$$

Here, M_1, M_2, u_1, and $u_2$denote the molar mass and sound velocities of component 1 and 2, respectively.

IV. Free Length Theory[41]

The Free Length Theory, rooted in Jacobson's concept, offers a framework for calculating the ultrasonic velocity in binary mixtures. Initially expressed as:

$$u = K/(L_f\rho^{\frac{1}{2}}) = KY/(2V_a\rho^{\frac{1}{2}}) \quad \ldots (40)$$

For binary mixtures, it takes the form:

$$u = K(x_1Y_1 + x_2Y_2)/2[V_M - (x_1V_{0.1} + x_2V_{0.2})]\rho^{1/2} \quad \ldots (41)$$

Here, Y is an adjustable parameter derived from the sound velocity of pure liquids using:

$$Y = 2V_a u\rho^{1/2}/K \quad \ldots (42)$$

In these equations, K denotes the temperature-dependent Jacobson's constant[42], V_a represents the available molar volume, reflecting the mixture's compactness and bonding strength and is calculated using the relation:

$$V_a = V_M - V_0 \quad \ldots (43)$$

By substituting equation (42) into equation (41) and rearranging, we obtain:

$$u_{flt} = \left\{\left[x_1(V_{M1} - V_{0.1})u_1\rho_1^{1/2}\right] + \left[x_2(V_{M2} - V_{0.2})u_2\rho_2^{1/2}\right]\right\}/[V_M - (x_1V_{0.1} + x_2V_{0.2})]\rho^{1/2} \quad \ldots (44)$$

This equation elucidates that, according to the Free Length Theory, the square root of the inverse of the adiabatic compressibility of the liquid mixture $\left(u\rho^{\frac{1}{2}}\right)$is the sum of the available volume fraction average of the square root of the inverse of the adiabatic compressibility of the individual components.

These theoretical speed of sound relations offer diverse mathematical models for estimating the speed of sound in binary liquid mixtures. Each equation represents a distinct approach and makes specific assumptions about the mixture's properties. The Junjie equation (36) incorporates molar mass, density, and speed of sound of the pure components. The Nomoto equation (37) introduces molar volume and Wada's constant, derived from the speed of sound. The ideal mixture relation (39) simplifies the calculation by considering only molar mass and sound velocities. Finally, the Free Length Theory (44) builds on Jacobson's theory and introduces the concept of available molar volume, reflecting the compactness and bonding strength within the mixture.

These equations equip researchers with valuable tools for estimating the speed of sound in binary liquid mixtures, with implications across various fields such as acoustics, materials science, and chemical engineering.

Mathematical Representation of Excess or Deviation Functions

The excess or deviation functions for binary mixtures are often expressed using the Redlich-Kister polynomial equation[43]. This equation offers a versatile approach for fitting deviations in properties. Its form is as follows:

$$(Y)^E = x_1(1 - x_1)\sum_{i=1}^{n} A_i(2x_1 - 1)^i \quad \ldots (45)$$

Here, Y^Erepresents the excess or deviation properties, while x_i denotes the mole fraction of the i^{th} component. The coefficients A_i are determined through the Redlich-Kister equation. Utilizing the fourth-order form of the equation minimizes the standard deviation in Y^E.

To assess the accuracy of the model, the standard deviation (σ) is calculated using the relation:

$$\sigma(Y) = \left[\frac{\sum(Y_{exp}^E - Y_{cal}^E)}{N-P}\right]^{\frac{1}{2}} \quad \ldots (46)$$

Here, Y_{exp}^E and Y_{cal}^E represents the experimental and calculated values of excess properties, respectively. N is the number of experimental points, and P is the number of parameters of the Redlich-Kister equation. The Redlich-Kister polynomial equation provides a robust framework for fitting these deviations and accurately describing the changes in properties resulting from mixing. Equation (45) for binary mixtures enables the calculation of excess or deviation properties based on the mole fractions of the components.

Results and Discussion

Density (ρ) and Excess Molar Volume (V_m^E)

The experimental findings on the density (ρ) and excess partial molar volume (V_m^E) of the binary mixtures composed of α-terpineol (1) withfluoro-, chloro-, and bromobenzene at temperatures of 303.15K, 308.15K, and 313.15K are presented in TableS3 of Supplementary data.Additionally, a graphical representation of V_m^E*versus* mole fraction (x_1) at 303.15K is depicted in Fig. 1. The fitting coefficients (A_0, A_1, A_2, A_3, A_4) obtained from the Redlich-Kister polynomial equation for V_m^E are

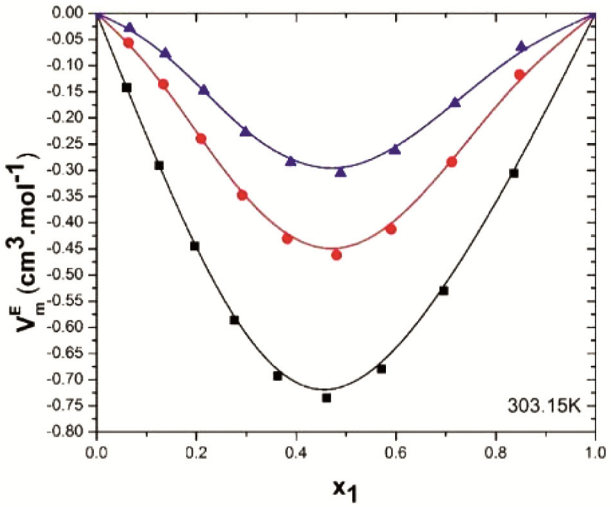

Fig. 1 — Excess molar volumes (V_m^E) for the system α-terpineol (1) + Fluoro–, Chloro–, and Bromo-benzene (2) as a function of mole fraction at T = 303.15K: ■, α-terpineol (1) + Fluorobenzene (2); ●, α-terpineol (1) + Chlorobenzene (2); ▲, α-terpineol (1) + Bromobenzene (2).

tabulated in Table S4 of supplementary data. Upon analysis of the V_m^E values presented in TableS3 of supplementary data, several noteworthy observations can be made:

- All binary mixtures exhibit negative values of V_m^E across all investigated temperatures.
- The negative V_m^E values tend to decrease with increasing temperature.
- The binary mixture of α-terpineol and fluorobenzene displays the highest negative V_m^E values, whereas the lowest negative values are observed in the binary mixture of α-terpineol and bromobenzene.

The maximum values of V_m^E for all binary mixtures at the studied temperatures are presented in the Table 1 below.

Further insight into the intermolecular interactions within the binary mixtures can be gleaned from the observed data. Notably, the α-terpineol + fluorobenzene binary mixture exhibits strong intermolecular interactions among present selected systems. Similar trends are observed in the other two mixtures containing chlorobenzene and bromobenzene, suggesting a consistent pattern of intermolecular behavior across the studied systems.

Further insight into the intermolecular interactions within the binary mixtures can be gleaned from the observed data. Notably, the α-terpineol + fluorobenzene binary mixture exhibits strong intermolecular interactions among present selected systems. Similar trends are observed in the other two mixtures containing chlorobenzene and bromobenzene, suggesting a consistent pattern of intermolecular behavior across the studied systems.

The weakening of these intermolecular interactions with increasing temperature can be attributed to the enhanced kinetic energy of the molecules, which reduces the propensity for strong molecular associations. Notably, the presence of the –OH group in α-terpineol offers additional opportunities for hydrogen bonding interactions within the binary mixtures. The oxygen atom in the –OH group possesses lone pairs, inducing a partial positive charge on the adjacent hydrogen atom. This highly polarized hydrogen atom can be engaged in stronger hydrogen bonding interactions with the electronegative halogen atom of the halobenzene molecules.

Table 1 — Maximum values of V_m^E for all binary mixtures

Binary Mixtures	Temperature (K)	Mole fraction (x_1)	V_m^E $(cm^3 \cdot mol^{-1})$
α-Terpineol + Fluorobenzene	303.15	0.4612	–0.7349
	308.15	0.4612	–0.6899
	313.15	0.4612	–0.6499
α-Terpineol + Chlorobenzene	303.15	0.4811	–0.4624
	308.15	0.4811	–0.4325
	313.15	0.4811	–0.4037
α-Terpineol + Bromobenzene	303.15	0.4889	–0.3054
	308.15	0.4889	–0.2843
	313.15	0.4889	–0.2693

Based on the observed interactions, the order of interaction strength between halobenzene and α-terpineol can be summarized as follows: Fluorobenzene>Chlorobenzene > Bromobenzene

The observed values of excess molar volume, V_m^E is due to blend of influences, each contributing to the observed behavior in binary mixtures. The manifestation of physical intermolecular forces, spanning from electrostatic interactions among charged atoms to dipole-dipole attractions, dipole-induced dipole interactions, and hydrogen bonding, predominantly steers the negative trend in V_m^E. These forces foster attractive interplays between molecules, culminating in a tighter arrangement and consequently, a negative excess molar volume. Conversely, certain repulsive interactions, often encountered between non-polar or polar molecules, may yield positive V_m^E values.

Moreover, disparities in geometry, structural attributes, and molar volume across the molecules in the binary mixture play a pivotal role. The geometric congruence between molecules facilitates a favorable accommodation of one component within the voids or recesses of another, contributing to a negative excess molar volume. This phenomenon arises from the synergistic interplay of structural and size compatibility between the molecules, fostering a denser arrangement and bolstering intermolecular interactions.

Hence, the amalgamation of these factors, encompassing intermolecular forces and geometrical attributes, collectively shapes the observed negative values of V_m^E [44-46].

In essence, the scrutiny of density and excess molar volume unravels profound insights into the intricate intermolecular dynamics within the α-terpineol and halobenzene binary mixtures. The presence of the –OH group inα-terpineol and electronegative halogen atom in halobenzene compounds nurtures robust intermolecular interactions, bonding, thereby engendering substantial negative values of V_m^E.

Infinite Dilution Partial Molar Volume ($\bar{V}^{o}_{m,i}$), Excess Partial Molar Volume ($\bar{V}^{o,E}_{m,i}$), Apparent Molar Volume ($V_{m,\Phi,i}$)

The calculated parameters, including Infinite dilution partial molar volume ($\bar{V}^{o}_{m,i}$), Excess partial molar volume ($\bar{V}^{o,E}_{m,i}$), and Apparent molar volume ($V_{m,\Phi,i}$), are detailed in Table S5 of supplementary data, with corresponding graphical representations depicted in Fig. 2 and Fig. 3, S1, and S2 of supplementary data. A comprehensive analysis of these values yields insightful observations:

- Negative values of $\bar{V}^{o,E}_{m,1}$ are consistently observed across all binary mixtures and temperatures.
- The magnitude of negative $\bar{V}^{o,E}_{m,1}$ decreases with temperature and across binary mixtures from fluorobenzene to bromobenzene.
- Remarkably, the apparent molar volume ($V_{m,\Phi,i}$) calculated through distinct methods demonstrates remarkable proximity.

The tabulated data in Table S5 of supplementary data further underscores the distinct intermolecular interactions of α-terpineol within different solvent environments. Particularly notable is the heightened interaction observed in fluorobenzene compared to chlorobenzene and bromobenzene.

Additionally, Table 2 and Figs. S3 to S6 of supplementary data presents the calculated values of infinite dilution apparent molar volume $\bar{V}^{o,E}_{m,1}$, limiting apparent molar expansibility (E^{o}_{Φ}), and empirical parameters S_v and B_v of the Redlich-Rosenberg-Mayer equation, along with their respective standard deviations (σ). It is noteworthy that:

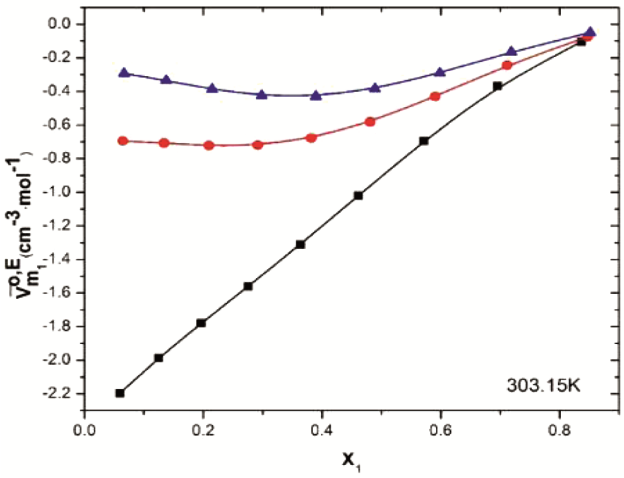

Fig. 2 — Infinite Dilution Excess Partial Molar Volume ($\bar{V}^{o,E}_{m_1}$)for the system α-terpineol (1) + Fluoro–, Chloro–, and Bromo-benzene (2) as a function of mole fraction at T = 303.15K: ■, α-terpineol (1) + Fluorobenzene (2); ●, α-terpineol (1) + Chlorobenzene (2); ▲, α-terpineol (1) + Bromobenzene (2).

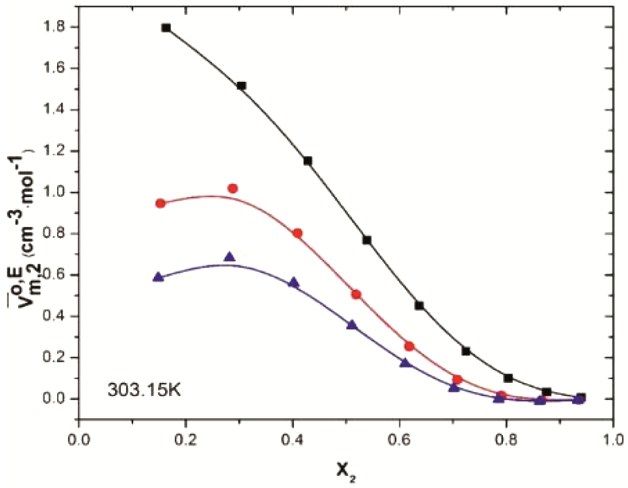

Fig. 3 — Infinite Dilution Excess Partial Molar Volume ($\bar{V}^{o,E}_{m_2}$)for the system α-terpineol (1) + Fluoro–, Chloro–, and Bromo-benzene (2) as a function of mole fraction at T = 303.15K: ■, α-terpineol (1) + Fluorobenzene (2); ●, α-terpineol (1) + Chlorobenzene (2); ▲, α-terpineol (1) + Bromobenzene (2).

Table 2 — Infinite dilution apparent molar volume,$V^{o}_{m,\Phi,1}$ Empirical parameters S_v and B_v of Redlich-Rosenberg-Mayer equation with standard deviation, σ and the limiting apparent molar expansibility, E^{o}_{Φ} for α-terpineol (1) + Fluoro–, Chloro– and Bromo benzene (2) at 303.15, 308.15 and 313.15K.

T (K)	$V^{o}_{m,\Phi,1}$(cm^3·mol^{-1})	S_v(cm^3·mol$^{-(3/2)}$·kg$^{(1/2)}$)	B_v(cm^3·mol^{-2}·kg)	σ	E^{o}_{Φ}(cm^3·mol^{-1}·K^{-1})
		α-terpineol (1) + Fluorobenzene (2)			
303.15	163.725	0.1039440	–0.001207640	0.89977	0.2220
308.15	164.827	0.0753307	–0.000783055	0.75273	0.2188
313.15	165.913	0.0486436	–0.000388434	0.64873	0.2156
		α-terpineol (1) + Chlorobenzene (2)			
303.15	165.051	0.0356691	–0.000298189	0.44026	0.1943
308.15	166.005	0.0167714	0.000006007	0.41321	0.1873
313.15	166.924	0.0025703	0.000226445	0.39873	0.1803
		α-terpineol (1) + Bromobenzene (2)			
303.15	165.535	0.0217847	–0.000137919	0.27426	0.1610
308.15	166.348	0.0122182	0.000059962	0.26364	0.1642
313.15	167.177	0.0011540	0.000299241	0.27034	0.1674

- Positive values of $V^{o}_{m,\Phi,1}$ are evident across all binary mixtures and temperatures. Particularly, the α-terpineol + fluorobenzene binary mixture exhibits the highest positive $V^{o}_{m,\Phi,1}$ value, indicative of strong intermolecular interactions between its components.
- Concurrently, the positive S_v values, negativeB_v parameter, and E^{o}_{Φ} values further corroborate the presence of robust intermolecular interactions.

These findings offer profound insights into the interplay of molecular forces within the studied binary mixtures, shedding light on their thermodynamic behavior and providing a basis for further exploration into their properties and applications.

Speed of Sound (u) and Deviation in Speed of Sound (Δu)

The comprehensive assessment of speed of sound (u) and its deviation (Δu) in various binary mixtures provides valuable insights into the intermolecular interactions governing their acoustic behavior. The experimental measurements of u and calculated values of Δu across different compositions and temperatures are compiled in TableS6 of supplementary data, with the deviation depicted graphically in Fig. 4. Notably, the fitting coefficients of the Redlich-Kister polynomial equation for Δu are detailed in Table S7 of supplementary data.

Key observations derived from the tabulated data are outlined as follows:

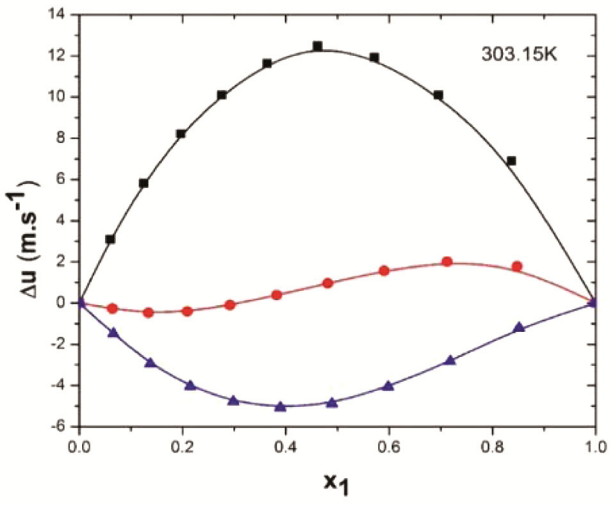

Fig. 4 — Deviation in speed of sound (Δu) for the system α-terpineol (1) + Fluoro–, Chloro–, and Bromo-benzene (2) as a function of mole fraction at T = 303.15K: ■, α-terpineol (1) + Fluorobenzene (2); ●, α-terpineol (1) + Chlorobenzene (2); ▲, α-terpineol (1) + Bromobenzene (2).

- The α-terpineol + fluorobenzene binary mixture consistently exhibits positive values of Δu across all temperatures. Interestingly, as the binary mixture transitions from fluorobenzene to bromobenzene, the positive deviation shifts towards negative values.
- A notable trend is observed with increasing temperature, wherein positive Δu values tend to become less positive, while negative Δu values become more negative.

The maximum values of Δu for all binary mixtures at the studied temperatures are presented in the Table 3.

Specifically, for the α-terpineol+ fluorobenzene binary mixture, the highest positive Δu value is noted. This observation underscores the strong intermolecular interactions between α-terpineol and fluorobenzene molecules, facilitating a closer orientation and efficient transmission of sound waves through the medium.

Furthermore, it is noteworthy that these interactions diminish with rising temperature, attributed to the increased kinetic energy of molecules, which disrupts the favorable alignment required for enhanced acoustic transmission[47,48].

This analysis offers valuable insights into the intricate interplay of molecular interactions governing the acoustic properties of binary mixtures, paving the way for a deeper understanding of their thermodynamic behavior and potential applications in various fields.

Theoretical Speed of Sound Relations

The analysis of theoretical speed of sound relations, including the Nomoto relation (u_{nmt}), Ideal mixture relation (u_{imr}), Junji relation (u_{junji}), and Free length theory relation (u_{flt}), offers insights into their accuracy in predicting speed of sound values. The average percentage deviation ($\sigma\%$) values for these relations

Table 3 — Maximum values of Δu for all binary mixtures.

Binary Mixtures	Temperature (K)	mole fraction (x_1)	Δu (m·s^{-1})
α-terpineol + Fluorobenzene	303.15	0.4612	12.49
	308.15	0.4612	11.32
	313.15	0.4612	10.31
α-terpineol + Chlorobenzene	303.15	0.1338	–0.48
		0.7120	2.02
	308.15	0.1338	–0.79
		0.7120	1.81
	313.15	0.1338	–1.13
		0.7120 / 0.8476	1.54 / 1.54
α-terpineol + Bromobenzene	303.15	0.3894	–5.08
	308.15	0.3894	–5.43
	313.15	0.3894	–5.79

across different binary mixtures are summarized in Table 4, facilitating comparative assessments.

Key observations derived from the analysis are outlined as follows:

For α-terpineol + fluorobenzene binary mixtures:

- The Junji relation (u_{junji}) exhibits the lowest σ% values at 303.15K, while the Free length theory (u_{flt}) relation displays the lowest σ% values at 303.15K and 313.15K.
- Conversely, the Ideal mixture relation (u_{imr}) demonstrates the highest σ% values across all studied temperatures.

For α-terpineol + chlorobenzene binary mixtures:

- The Junji relation (u_{junji}) shows the lowest σ% values at 303.15K and 308.15K, while the Nomoto relation (u_{nmt}) exhibits the lowest σ% values at 313.15K.
- In contrast, the Ideal mixture relation (u_{imr}) yields the highest σ% values across all studied temperatures.

For α-terpineol + bromobenzene binary mixtures:

- The Junji relation (u_{junji}) consistently demonstrates the lowest σ% values across all studied temperatures.
- Conversely, the Nomoto relation (u_{nmt}) consistently yields the highest σ% values at all studied temperatures.

These observations highlight the varying degrees of accuracy among the theoretical speed of sound relations for different binary mixtures and temperatures. Such insights are valuable for understanding the predictive capabilities of these relations in estimating speed of sound values in binary mixtures.

Table 4 — Average Percentage Deviation (σ%) in the Speed of sound from Various Theoretical Relations for α-terpineol + Fluoro-, Chloro- and Bromo benzene Mixtures at 303.15, 308.15 and 313.15K.

Theoretical Relations	T (K)		
	303.15	308.15	313.15
α-terpineol (1) + Fluorobenzene (2)			
u_{nmt}	1.14532	1.24326	1.34152
u_{imr}	5.27859	5.30648	5.17881
u_{junji}	0.49541	0.55177	0.85299
u_{flt}	0.64633	0.50765	0.41422
α-terpineol (1) + Chlorobenzene (2)			
u_{nmt}	0.92111	0.95331	0.99053
u_{imr}	1.95416	1.95966	1.96483
u_{junji}	0.72628	0.75485	1.00494
u_{flt}	1.65018	1.46789	1.32969
α-terpineol (1) + Bromobenzene (2)			
u_{nmt}	1.76572	1.79681	1.82947
u_{imr}	0.86704	0.84723	0.83203
u_{junji}	0.61098	0.64277	0.67571
u_{flt}	1.62832	1.52517	1.44715

nmt = Nomoto, imr = Ideal mixture relation, junji= junji, flt = Free length Theory

Isentropic Compressibility ($\mathbf{k_s}$), Deviation in Isentropic Compressibility ($\mathbf{\Delta k_s}$), Acoustical Impedance ($\mathbf{z}$), Deviation in Acoustical Impedances ($\mathbf{\Delta z}$), and Intermolecular Free Length ($\mathbf{L_f}$)

The investigation into isentropic compressibility (k_s), deviation in isentropic compressibility (Δk_s), acoustical impedance (z), deviation in acoustical impedances (Δz), and intermolecular free length (L_f) across various binary mixtures yields crucial insights into their acoustic characteristics. Tabulated data encompassing these properties across different compositions and temperatures are presented in Tables S8, S11 of supplementary data, and Table 5,

Table 5 — Intermolecular Free Length (L_f) *vs* Mole Fraction (x_1) for α-terpineol + Fluoro-, Chloro- and Bromo benzene Mixtures at 303.15, 308.15 and 313.15K.

x_1	L_f (A^0)		
	303.15 K	308.15 K	313.15 K
α-terpineol (1) + Fluorobenzene (2)			
0.0000	19.3930	19.7433	20.1010
0.0596	19.2364	19.5844	19.9395
0.1249	19.0746	19.4196	19.7688
0.1965	18.9063	19.2442	19.5879
0.2756	18.7314	19.0600	19.3975
0.3634	18.5469	18.8690	19.1973
0.4612	18.3537	18.6683	18.9865
0.5711	18.1544	18.4604	18.7691
0.6954	17.9445	18.2415	18.5395
0.8370	17.7211	18.0078	18.2963
1.0000	17.4943	17.7653	18.0382
α-terpineol (1) + Chlorobenzene (2)			
0.0000	18.5687	18.8749	19.1860
0.0643	18.4956	18.8012	19.1113
0.1338	18.4168	18.7202	19.0283
0.2094	18.3303	18.6308	18.9356
0.2918	18.2356	18.5329	18.8343
0.3820	18.1328	18.4265	18.7244
0.4811	18.0213	18.3114	18.6050
0.5905	17.9008	18.1866	18.4759
0.7120	17.7713	18.0526	18.3369
0.8476	17.6346	17.9108	18.1895
1.0000	17.4943	17.7653	18.0382
α-terpineol (1) + Bromobenzene (2)			
0.0000	19.4544	19.7619	20.0750
0.0662	19.3162	19.6234	19.9358
0.1375	19.1694	19.4747	19.7849
0.2147	19.0104	19.3127	19.6203
0.2983	18.8390	19.1386	19.4420
0.3894	18.6537	18.9492	19.2488
0.4889	18.4536	18.7450	19.0397
0.5981	18.2370	18.5246	18.8148
0.7184	18.0047	18.2870	18.5722
0.8516	17.7559	18.0332	18.3129

with graphical representations provided in Fig. 5 and Fig. 6. Additionally, the Redlich-Kister polynomial equation's fitting coefficients for Δk_s and Δz are elucidated in Tables S9 and S12 of supplementary data, respectively.

Noteworthy observations derived from the analysis are highlighted as follows:

- The α-Terpineol + fluorobenzene binary mixture consistently exhibits negative values of Δk_s across all temperatures. As the binary mixture changes from fluorobenzene to bromobenzene, the negative deviation shifts towards positive values.
- Similarly, the α-Terpineol + fluorobenzene binary mixture demonstrates positive Δz values across all temperatures. However, as the binary mixture changes from fluorobenzene to bromobenzene, the positive deviation shifts towards negative values.
- A notable trend observed with increasing temperature is the decrease in positive Δz values and negative Δz values become more negative.

The maxima/minima values of Δk_s and Δz for all binary mixtures at the studied temperatures are presented in Table 6.

Specifically, the α-Terpineol + fluorobenzene binary mixture exhibits the highest positive Δu value due to strong intermolecular interactions between fluorobenzene and α-Terpineol molecules, strengthening a closer molecular orientation. The Δk_s values are negative which also indicates for strong intermolecular interactions. These negative deviations shift towards positive values as intermolecular interactions diminish between binary mixture components.

Similarly, the positive Δz values for the α-Terpineol + fluorobenzene binary mixture gradually shift towards more negative values with decreasing

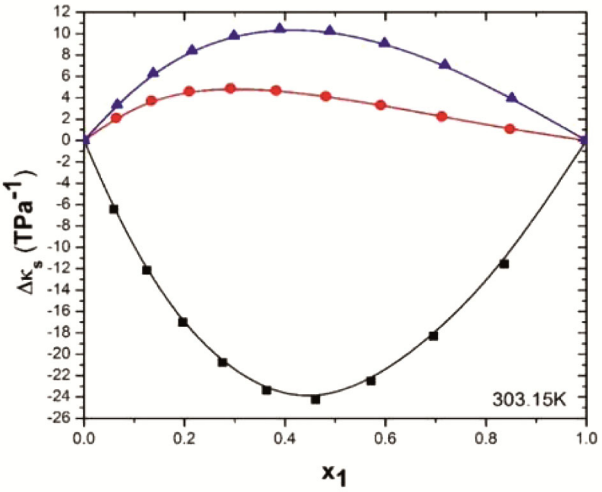

Fig. 5 — Deviation in isentropic compressibility (Δk_s) for the system α-terpineol (1) + Fluoro–, Chloro–, and Bromo-benzene (2) as a function of mole fraction at T = 303.15K: ■, α-terpineol (1) + Fluorobenzene (2); ●, α-terpineol (1) + Chlorobenzene (2); ▲, α-terpineol (1) + Bromobenzene (2).

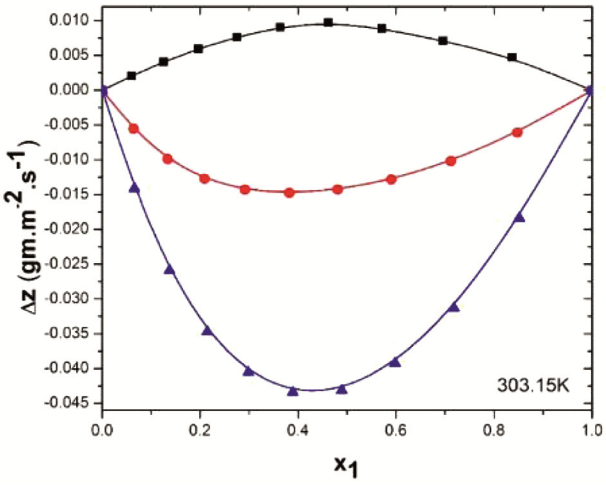

Fig. 6 — Deviation in acoustical impedance (Δz) for the system α-terpineol (1) + Fluoro–, Chloro–, and Bromo-benzene (2) as a function of mole fraction at T = 303.15K: ■, α-terpineol (1) + Fluorobenzene (2); ●, α-terpineol (1) + Chlorobenzene (2); ▲, α-terpineol (1) + Bromobenzene (2).

Table 6 — Maxima/minima values of Δk_s and Δz for all binary mixtures.

Binary Mixtures	Temperature(K)	mole fraction (x_1)	Δk_s (TPa^{-1})	mole fraction (x_1)	Δz (g·m^{-2}·s^{-1}) × 10^{-3}
α-terpineol + Fluorobenzene	303.15	0.4612	–24.26	0.4612	0.0097
	308.15	0.4612	–25.02	0.4612	0.0085
	313.15	0.4612	–26.09	0.4612	0.0075
α-terpineol + Chlorobenzene	303.15	0.2918	4.87	0.3820	–0.0148
	308.15	0.2918	5.36	0.3820	–0.0149
	313.15	0.2918	5.92	0.3820	–0.0152
α-terpineol + Bromobenzene	303.15	0.3894	10.44	0.3894	–0.0434
	308.15	0.3894	11.20	0.3984	–0.0433
	313.15	0.3894	11.97	0.3894	–0.0430

intermolecular interaction strength which is consistent with the observed trends in Δk_s values.

Furthermore, the observed intermolecularfree length (L_f) values for all binary mixtures is adding more support for the variations observed in above said intermolecular interactions.

Infinite Dilution Partial Molar Isentropic Compressibility ($\bar{K}^{o}_{s,m,i}$), Excess Partial Molar Isentropic Compressibility ($\bar{K}^{o,E}_{s,m,i}$), and Apparent Molar Isentropic Compressibility ($K_{s,m,\Phi,i}$)

The exploration of infinite dilution partial molar isentropic compressibility ($\bar{K}^{o}_{s,m,i}$), excess partial molar isentropic compressibility ($\bar{K}^{o,E}_{s,m,i}$), and apparent molar isentropic compressibility ($K_{s,m,\Phi,i}$) across various binary mixtures provides valuable insights into their intermolecular interactions. These values, calculated for all binary mixtures across different temperatures, are tabulated in Table S10 of supplementary data, accompanied by graphical representations showed in Fig. 7, Fig. 8, and S7 to S12of supplementary data. Furthermore, the fitting coefficients of the Redlich-Kister polynomial equation for $K^{E}_{s,m}$ are detailed in Table S9 of supplementary data.

Key observations derived from the analysis are summarized as follows:

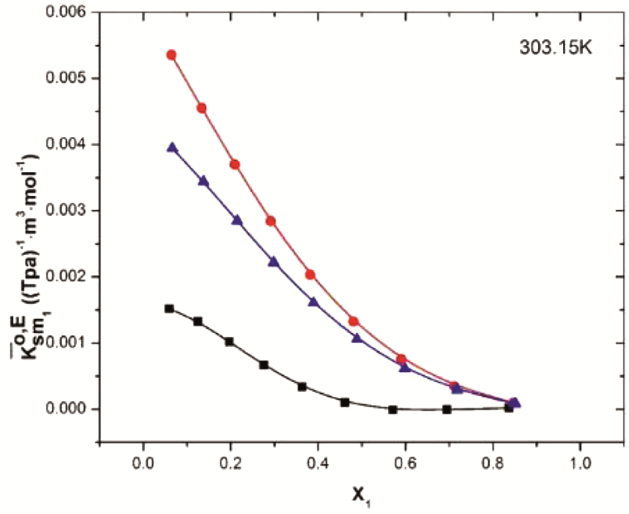

Fig. 7 — Infinite Dilution Excess Partial Molar Isentropic Compressibility ($\bar{K}^{o,E}_{s,m_1}$)for the system α-terpineol (1) + Fluoro–, Chloro–, and Bromo-benzene (2) as a function of mole fraction at T = 303.15K: ■, α-terpineol (1) + Fluorobenzene (2); ●, α-terpineol (1) + Chlorobenzene (2); ▲, α-terpineol (1) + Bromobenzene (2).

- Across all studied temperatures, all binary mixtures exhibit positive values of $\bar{K}^{o,E}_{s,m,1}$ and negative values of $\bar{K}^{o,E}_{s,m,2}$.
- With increasing temperature, the positive values of $\bar{K}^{o,E}_{s,m,1}$ rise, while the negative values of $\bar{K}^{o,E}_{s,m,2}$ become more negative.

These observations suggest that fluorobenzene molecules display the highest intermolecular interaction with α-terpineolmolecules among the binary mixtures studied.

Additionally, the table detailing the calculated values of infinite dilution apparent molar isentropic compressibility ($K^{o}_{s,m,\Phi,1}$) with empirical parameters S_k and B_k of the Redlich-Rosenberg-Mayer equation, along with standard deviation (σ), offers further insights. It is evident from Table 7 that all binary mixtures manifest positive values of $K^{o}_{s,m,\Phi,1}$, which increase with temperature and changefrom fluorobenzene to bromobenzene binary mixtures. This indicates the presence of the strongest intermolecular interactions in fluorobenzene binary mixtures, with interaction strength diminishing with increasing temperature and transitioning to bromobenzene binary mixtures. The large negative values of S_k and positive values of B_k parameters suggest the prevalence of electrostatic-type interactions in binary mixtures, where the positive values of $K^{o}_{s,m,\Phi,1}$ indicate a higher solvent intrinsic compressibility effect compared to the penetration effect[49-51].

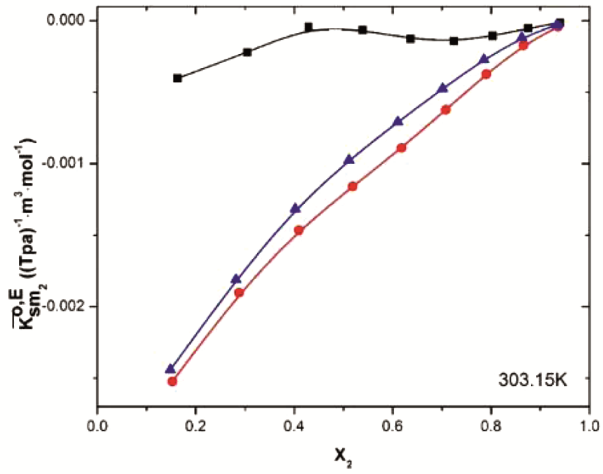

Fig. 8 — Infinite Dilution Excess Partial Molar Isentropic Compressibility ($\bar{K}^{o,E}_{s,m_2}$) for the system α-terpineol (1) + Fluoro–, Chloro–, and Bromo-benzene (2) as a function of mole fraction at T = 303.15K: ■, α-terpineol (1) + Fluorobenzene (2); ●, α-terpineol (1) + Chlorobenzene (2); ▲, α-terpineol (1) + Bromobenzene (2).

Table 7 — Infinite dilution apparent molar isentropic compressibility, $K^{o}_{s,m,\Phi,1}$, Empirical parameters S_k and B_k of Redlich-Rosenberg-Mayer equation with standard deviation, σ, for α-terpineol + Fluoro–, Chloro– and Bromo benzene Mixtures at 303.15, 308.15 and 313.15K.

T (K)	$K^{o}_{s,m,\Phi,1}$(m^{-3}·(TPa)$^{-1}$·mol^{-1})	S_k(m^{-3}·(TPa)$^{-1}$·$mol^{-(3/2)}$·$kg^{(1/2)}$)	B_k(m^{-3}·(TPa)$^{-1}$·mol^{-2}·kg)	σ
		α-terpineol (1) + Fluorobenzene (2)		
303.15	0.091566100	–0.000076208	0.000001064	0.00058
308.15	0.096147800	–0.000177155	0.000002535	0.00134
313.15	0.100880000	–0.000282117	0.000004057	0.00210
		α-terpineol (1) + Chlorobenzene (2)		
303.15	0.095102600	–0.000300837	0.000004419	0.00201
308.15	0.099056000	–0.000360775	0.000005340	0.00241
313.15	0.103142000	–0.000418947	0.000006215	0.00280
		α-terpineol (1) + Bromobenzene (2)		
303.15	0.094139500	–0.000291832	0.000005599	0.00137
308.15	0.097855500	–0.000345235	0.000006683	0.00161
313.15	0.101746000	–0.000405927	0.000007935	0.00188

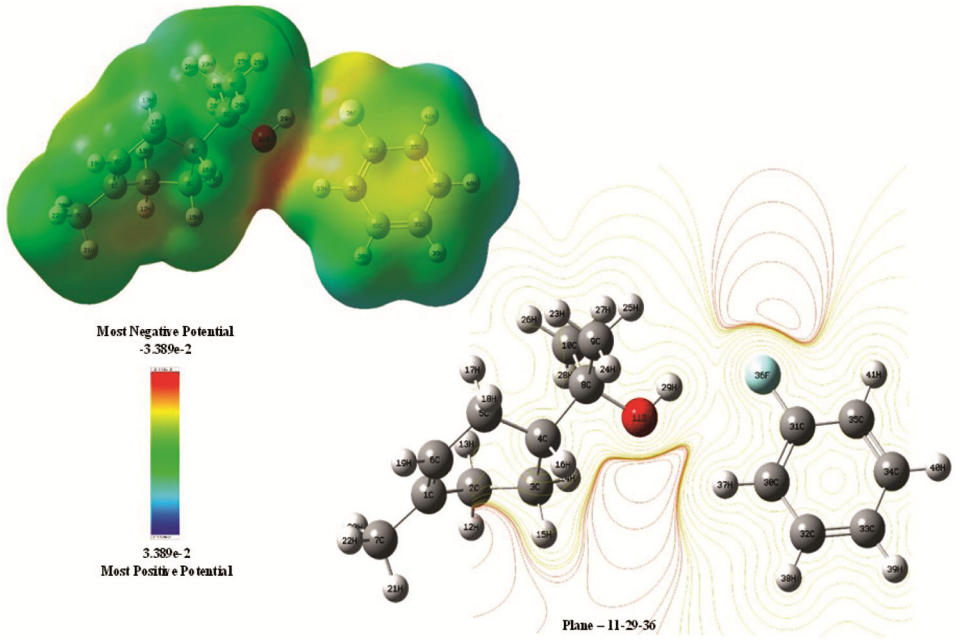

Fig. 9 — Optimized geometric structure of α-terpineol + Fluorobenzene (First Possible Interaction site) with 3D MESP and 2D electrostatic potential contour map based on B3LYP/6-31+G(d,p) at 298.15K.

From the foregoing discussion, it can be inferred that the strength of interaction of halobenzene with α-terpineol follows the order: Fluorobenzene> Chlorobenzene> Bromobenzene.

Computational Analysis

Geometry Optimisation and Mulliken Charge Analysis:

The bond lengths (Å) between atoms and Mulliken charges of pure α-terpineol, halobenzenes, and their binary mixtures at 298.15K are presented in Tables S13 and S14 of supplementary data. Optimized structures of pure components and their binary mixtures, including Mulliken charges, 3D Molecular Electrostatic Potential (3D-MESP), 2D Electrostatic Potential Contour Map (ESPCM), and solvation states of α-terpineol with halobenzene (fluorobenzene, chlorobenzene, and bromobenzene), along with their respective Mulliken charges, 3D-MESP, and 2D-ESPCM, are illustrated in Fig. 9, Fig. 10, and S13 to S18of supplementary data.

Observations drawn from the tables and figures for pure components are as follows:

α-Terpineol

In the optimized structure of α-terpineol, the –OH group exhibits the potential to act as a proton donor (electron density acceptor). The hydrogen atom H29 possesses the highest positive charge of 0.333091 due

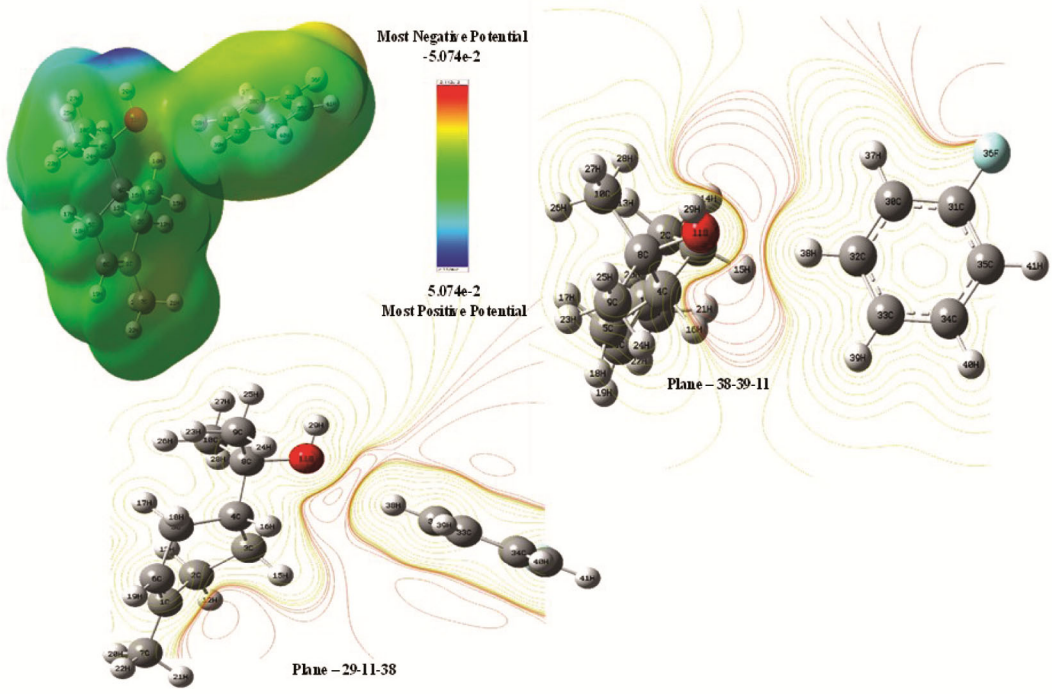

Fig. 10 — Optimized geometric structure of α-terpineol + Fluorobenzene (Second Possible Interaction site) with 3D MESP and 2D electrostatic potential contour map based on B3LYP/6-31+G(d,p) at 298.15K.

to the presence of lone pairs containing the oxygen atom O11, which carries a negative charge of –0.503554 (refer to Fig. S15of supplementary data). Other hydrogen atoms, excluding those present in –OH group, also exhibit positive charges, suggesting possible dipole-dipole and dipole-induced dipole interactions with electronegative atoms of the solvent in binary mixture states.

Halobenzenes

In halobenzenes, the halogen atoms possess an excess negative charge, while the hydrogen atoms attached to the aromatic ring's carbons carry some positive charge (refer to Fig. S16 to S18 of supplementary data).

Considering the fore mentioned properties of pure components, there are possibilities of dipole-dipole, dipole-induced dipole, and primarily hydrogen bonding between electropositive atoms and lone pairs containing electronegative atoms of α-terpineol and halobenzenes.

Interactions in Binary Mixtures

Based on the charges and electron density on atoms, several possible interaction sites between α-terpineol and halobenzenes can be identified. Among them, two main possible interaction sites are:

First possible interaction site

- Interaction between lone pairs containing electronegative oxygen atom O11 of α-terpineol molecule and electropositive hydrogen atom H37 of fluorobenzene.
- Interaction between the highly electronegative fluorine atom of fluorobenzene and the highly positive hydrogen atom H29 of α-terpineol molecule.

Second possible interaction site

- Interaction between lone pairs containing oxygen atom O11 of α-terpineol molecule and hydrogen atom H39 of halobenzene (hydrogen atoms distant from the fluorine atom).

In the present study, possible interaction sites are calculated only for the α-terpineol + fluorobenzene binary mixture. Similar results are expected for binary mixtures containing chlorobenzene and bromobenzene, with variations attributable only to the halogen atom, whose effects can also be understood from primary and secondary calculated properties.

A review of Tables S13 and S14 of supplementary data reveals strong hydrogen bonding between O11 and H37, as well as between H29 and F36 atoms in the first possible interaction site. In this site, the lone pair containing oxygen O11 forms a new hydrogen

bond by donating electron density to the C30–H37 bond. As a result, the Mulliken charge value of O11 changes from –0.503554 (in the pure state) to –0.402112 (in the binary mixture state), indicating a decrease in the Mulliken charge value of O11.

Similarly, the electronegatively charged fluorine atom acts as a proton acceptor, and the H29 atom acts as a proton donor. Thus, the fluorine atom interacts with the H29 atom by donating electron density from F36 to the O11–H29 bond. This donation of electron density alters the Mulliken charge value from –0.49146 (in the pure state) to –0.360355 (in the binary mixture state). Changes in the Mulliken charge values and bond lengths (Å) in the solvation study using the Polarizable Continuum Model (PCM) method also supports the presence of hydrogen bonding and as discussed earlier.

Natural Bond Orbital (NBO) Analysis

Second-order perturbation energy calculations of Natural Bond Orbital (NBO) analysis further support the presence of intermolecular interactions between different atoms of components in binary mixtures. Detailed values of energies associated with different interactions are presented in Table 8, with some discussed as follows:

α-Terpineol + Fluorobenzene - First possible interaction site

Interaction from α-terpineol to fluorobenzene

- Interaction between $\sigma_{O11-H29} \rightarrow \sigma^*_{C30-H37}$ with an energy value of 0.12 $KJ \cdot mol^{-1}$.
- Interaction between O11 lone pair (1) $\rightarrow \sigma^*_{C30-H37}$ with an energy value of 1.24 $KJ \cdot mol^{-1}$.
- Interaction between O11 lone pair (3) $\rightarrow \sigma^*_{C30-H37}$ with an energy value of 0.21 $KJ \cdot mol^{-1}$.

Interaction from fluorobenzene to α-terpineol

- Interaction between $\sigma_{C30-H37} \rightarrow \sigma^*_{C8-O11}$ with an energy value of 0.12 $KJ \cdot mol^{-1}$.
- Interaction between F36 lone pair (1) $\rightarrow \sigma^*_{O11-H29}$ with an energy value of 0.66 $KJ \cdot mol^{-1}$.
- Interaction between F36 lone pair (2) $\rightarrow \sigma^*_{O11-H29}$ with an energy value of 2.13 $KJ \cdot mol^{-1}$.

α-Terpineol + Fluorobenzene - Second possible interaction site

Interaction from α-terpineol to fluorobenzene

- Interaction between O11 lone pair (1) $\rightarrow \sigma^*_{C32-H38}$ with an energy value of 2.40 $KJ \cdot mol^{-1}$.

Table 8 — Second order perturbation energies (E(2)/$KJ \cdot mol^{-1}$) of hydrogen bonds and interactions for obtained by NBO calculation using B3LYP/6-31+G(d,p).

Association	Donor NBO (i)	Acceptor NBO (j)	E(2)/ $KJ \cdot mol^{-1}$
α-terpineol (1) + Fluorobenzene (2)			
First Possible Interaction Site			
From Unit 1 to Unit 2 (α-terpineol to Fluorobenzene)			
1	BD (1) C8-O11	RY*(1) H37	0.42
2	BD (1) O11-H29	RY*(1) H37	0.10
3	BD (1) O11-H29	BD*(1) C30-H37	0.12
4	LP (1) O11	BD*(1) C30-H37	1.24
5	LP (2) O11	BD*(1) C30-H37	0.21
From Unit 2 to Unit 1 (Fluorobenzene to α-terpineol)			
1	BD (1) C30 - H37	RY*(3) O11	0.10
2	BD (1) C30 - H37	RY*(4) O11	0.08
3	BD (1) C30 - H37	BD*(1) C8-O11	0.12
4	LP (1) F36	BD*(1) O11-H29	0.66
5	LP (2) F36	BD*(1) O11-H29	2.13
Second Possible Interaction Site			
From Unit 1 to Unit 2 (α-terpineol to Fluorobenzene)			
1	BD (1) C8-O11	RY*(1) H38	0.53
2	LP (1) O11	RY*(1) H38	0.05
3	LP (1) O11	BD*(1) C32-H38	2.40
4	LP (2) O11	BD*(1) C32-H38	0.12
From Unit 2 to Unit 1 (Fluorobenzene to α-terpineol)			
1	BD (1) C32-H38	RY*(2) O11	0.12
2	BD (1) C32-H38	RY*(3) O11	0.08
3	BD (1) C32-H38	BD*(1) C8-O11	0.08

Threshold for printing:0.50 kcal/mol
(Intermolecular threshold: 0.05 kcal/mol)

- Interaction between O11 lone pair (1) $\rightarrow \sigma^*_{C32-H38}$ with an energy value of 0.12 $KJ \cdot mol^{-1}$.

Interaction from fluorobenzene to α-terpineol

- Interaction between $\sigma_{C32-H38} \rightarrow \sigma^*_{C8-O11}$ with an energy value of 0.08 $KJ \cdot mol^{-1}$.

Noncovalent Interactions (NCI) and Reduced Density Gradient (RDG) Analysis

The non-covalent interactions (NCI) and reduced density gradient (RDG) analysis were carried out to

understand the intermolecular interactions within our binary mixtures. This theoretical approach offers a detailed visualization of molecular interactions, distinguishing various types of weak forces such as hydrogen bonds, van der Waals interactions, and repulsive steric interactions.

The NCI methodis used to characterize and evaluate the nature of intermolecular interactions. This method is grounded in the concept of the reduced density gradient (RDG), an important dimensionless quantity in Density Functional Theory (DFT) that describes deviations from a uniform electron distribution. The RDG(r) function, denoted as s, is defined by the relationship:

$$s = \frac{1}{2(3\pi^2)^{1/3}} \frac{|\nabla\rho(r)|}{\rho(r)^{4/3}} \quad \ldots (47)$$

where $\rho(r)$ represents the electron density and $\nabla\rho(r)$ its gradient.

The type and nature of interactions can be inferred from the sign of the second eigenvalue of the Hessian matrix (λ_2). This provides insights into both bonded and non-bonded interactions. Specifically, higher electron density values at the interaction sites correlate with stronger interactions. By plotting RDG against theelectron density, regions of non-covalent interactions can be identified. When RDG approaches zero, the peaks in the plot of $s(r)$*versus* $sign(\lambda_2)\rho$ highlight the essential characteristics of these interactions.

The parameter $sign(\lambda_2)\rho$, where λ_2 is the second Hessian eigenvalue, serves as a crucial index in the NCI-RDG formalism, indicating the type of interaction:

- $sign(\lambda_2)\rho$<0 suggests attractive interactions (such as van der Waals forces and hydrogen bonds).
- $sign(\lambda_2)\rho$>0 indicates repulsive interactions (such as steric hindrance)[52,53].

The plots of Reduced Density Gradient (RDG) *versus* $sign(\lambda_2)\rho$ for the first and second possible interaction sites are presented in Fig. 11. In the RDG plot for the first possible interaction site, three attractive interaction spikes are observed between 0 and –0.02 (a.u.) values of $sign(\lambda_2)\rho$, highlighted in green. These spikes indicate attractive interactions between atoms such as O11, H37, F36, and H29 within the α-terpineol and fluorobenzene binary mixture.

Similarly, five repulsive interaction spikes are observed between 0 and 0.02 (a.u.) values of $sign(\lambda_2)\rho$, highlighted in red, indicating steric hindrance between atoms in the ring structure.

For the second possible interaction site, the RDG plot shows three attractive interaction spikes highlighted in green and four repulsive interaction spikes highlighted in red. Comparing both RDG plots, the first possible interaction site exhibits stronger attractive interactions between the involved atoms and functional groups than those in the second possible interaction site.

The Noncovalent Interaction (NCI) plots and NCI isosurface (at s = 0.5) with Electron Localization Function (ELF) maps for the first and second possible interaction sites of the α-terpineol and fluorobenzene binary mixture are shown in Fig. 12 and Fig. 13, respectively.

In Fig. 12, the green-colored NCI isosurface in the three-dimensional space between atoms O11, H37, F36, and H29 indicates the presence of attractive intermolecular interactions between these functional groups. Conversely, the red-colored NCI isosurface in the same optimized geometrical structure indicates

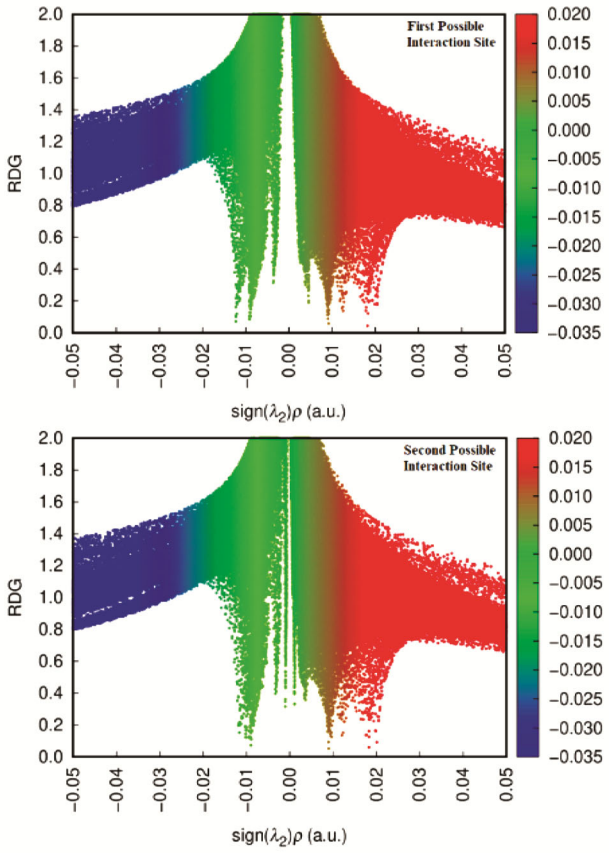

Fig. 11 — Plots of the Reduced Density Gradient (RDG) *versus* the electron density (ρ) multiplied by the sign of the second density Hessian eigenvalue (λ_2) at B3LYP/6-31+G(d,p) level of the theory for first and second possible interaction sites of α-terpineol (1) + Fluorobenzene (2) binary mixture.

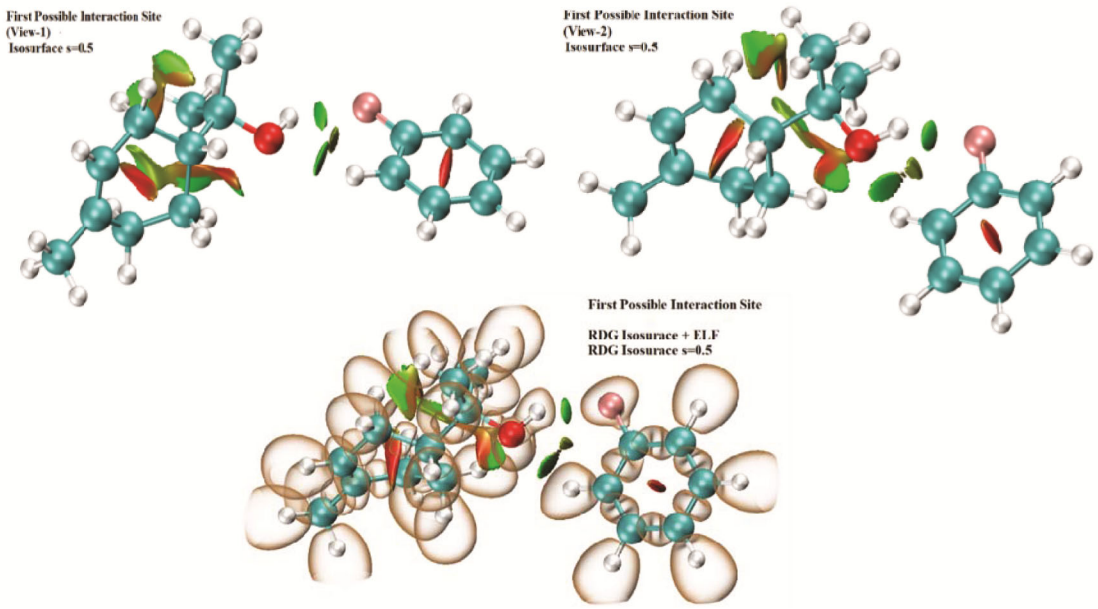

Fig. 12 — Non-Covalent Interaction (NCI) plots and NCI isosurface with Electron Localization Function (ELF) map of calculated geometry of first possible interaction sites of α-terpineol (1) + Fluorobenzene (2) binary mixture at B3LYP/6-31+G(d,p) level.

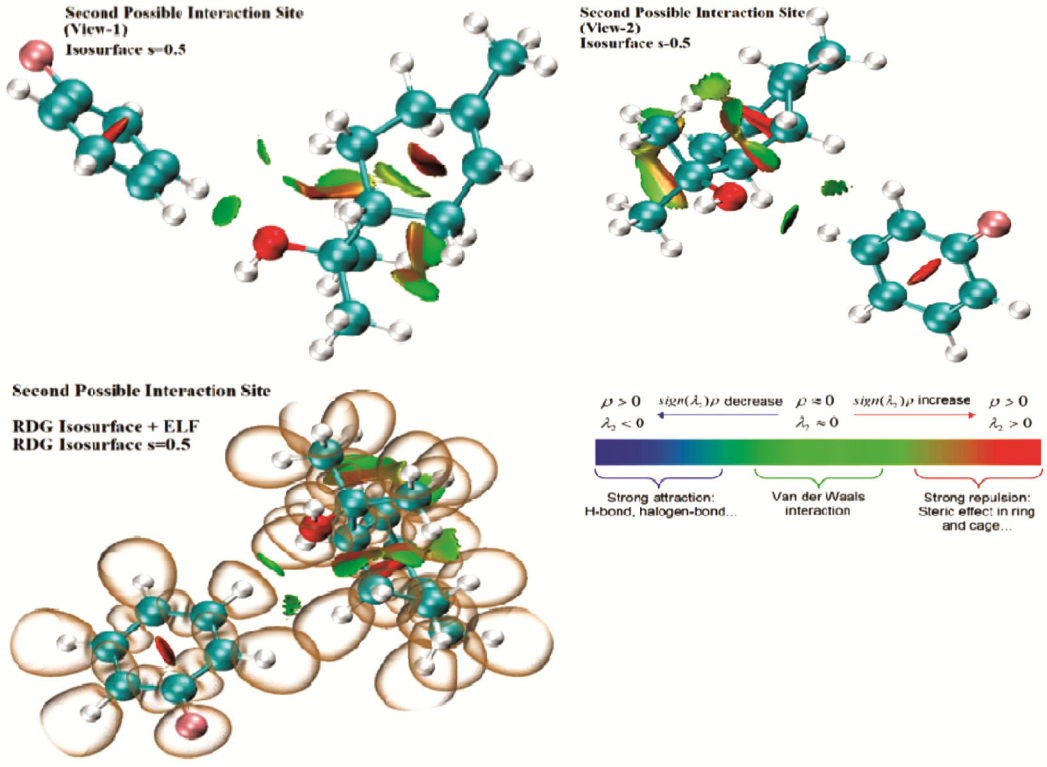

Fig. 13 — Non-Covalent Interaction (NCI) plots and NCI isosurface with Electron Localization Function (ELF) map of calculated geometry of second possible interaction sites of α-terpineol (1) + Fluorobenzene (2) binary mixture at B3LYP/6-31+G(d,p) level.

steric hindrance and repulsion, particularly at the atoms involved in the ring structure. Similar observations are made in Fig. 13 for the second possible interaction site.

In our study, NCI-RDG analysis proved effective in identifying weak interactions and allows for a clear visualization of interaction regions in real space, offering a comprehensive understanding of the

molecular interactions in our binary mixtures of α-terpineol and halobenzenes.

Electron Localization Function (ELF) and Localized Orbital Locator (LOL) Analyses

To further elucidate the nature of covalent bonding in our binary mixtures, the Electron Localization Function (ELF) and Localized Orbital Locator (LOL) analyses were carried out. These surface analyses provide insight into the electronic environment around atoms and the distribution of electron pairs on molecular surfaces[54,55].

The Electron Localization Function (ELF) map, shaded relief map with projection effects of the ELF, and Localized Orbital Locator (LOL) maps for the calculated geometries of the first and second possible interaction sites are depicted in Fig. 14 and Fig. 15, respectively.

ELF and LOL maps were generated to visualize the electronic localization and the behavior of localized orbitals in our mixtures. Both ELF and LOL are dependent on kinetic energy density, but they serve slightly different purposes. ELF is derived from electron pair density, highlighting regions of high electron localization, whereas LOL illustrates the gradient of localized orbitals, particularly when these orbitals overlap.

In our study, the ELF maps were constructed within a range from 0.0 to 1.0. Regions with delocalized electrons are represented by values below 0.5, while areas with highly localized electrons, often indicating covalent bonds or nuclear layers, exceed 0.5. These high localization regions are depicted in blue, highlighting significant electronic interactions and bonding regions.

The analysis revealed critical points and trajectories of chemical bonds, especially around hydrogen atoms, which are predominantly shown in red and orange areas on the ELF maps. These regions indicate significant chemical interactions, with electron density often surpassing the upper limit of the color scale (0.80), particularly in the central regions of some hydrogen atoms.

Our findings, illustrated through color tint maps and contour maps, demonstrate a clear localization of electrons around hydrogen atoms, consistent across all substances in the study. This high electron density in the nuclear region confirms the presence of strong covalent bonding and significant electronic interactions within our binary systems.

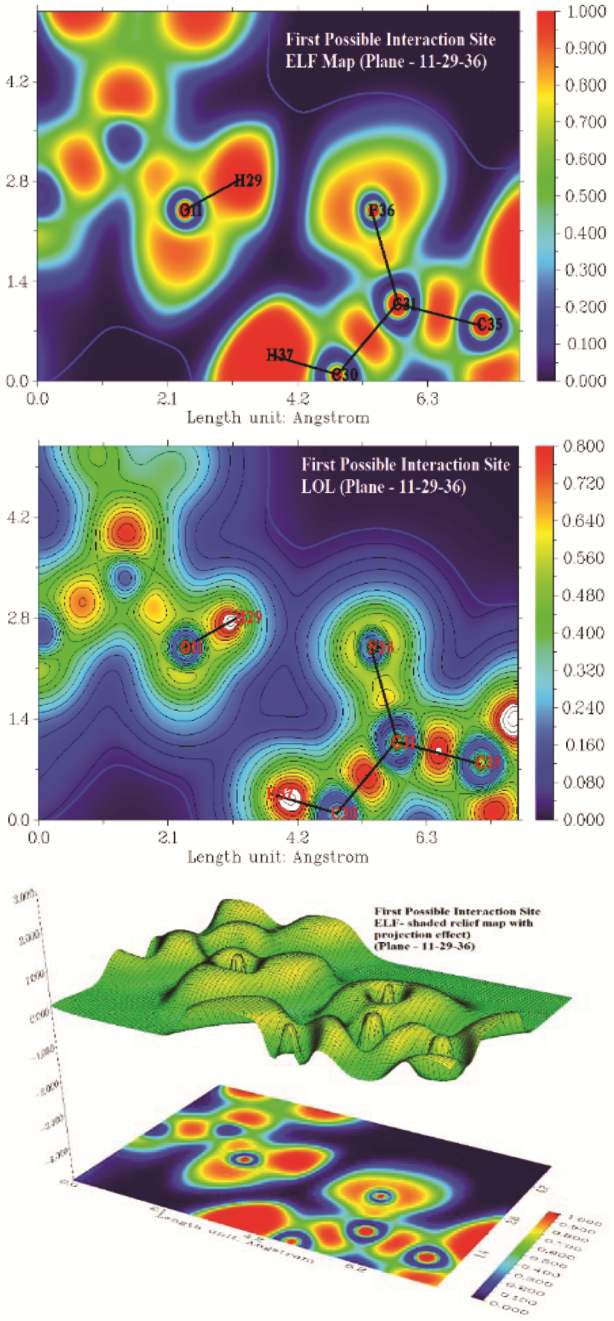

Fig. 14 — Electron Localization Function (ELF) map, Shaded relief map with projection effect of Electron Localization Function (ELF) and Localized Orbital Locator (LOL) map of calculated geometry of first possible interaction sites of α-terpineol (1) + Fluorobenzene (2) binary mixture at B3LYP/6-31+G(d,p) level.

These ELF and LOL analyses provide a detailed understanding of the covalent bonding nature and the electronic environment in our binary mixtures, offering a comprehensive visualization of the molecular interactions at play.

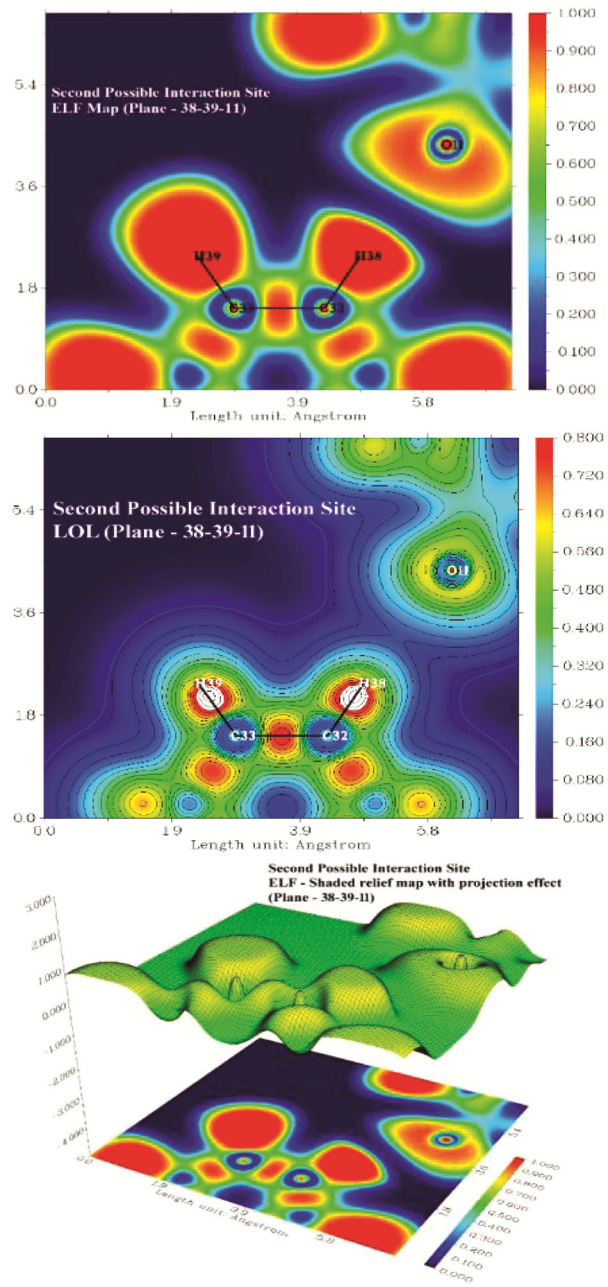

Fig. 15 — Electron Localization Function (ELF) map, Shaded relief map with projection effect of Electron Localization Function (ELF) and Localized Orbital Locator (LOL) map of calculated geometry of second possible interaction sites of α-terpineol (1) + Fluorobenzene (2) binary mixture at B3LYP/6-31+G(d,p) level.

By examining the Mulliken charges, bond lengths, MESP analysis, and NBO analysis, we corroborated the presence of significant intermolecular interactions, particularly hydrogen bonding. These interactions influence the physical properties of the mixtures, as evident from the variations in Mulliken charge values and bond lengths upon formation of the binary mixtures.

The computational analysis thus confirms the presence of strong hydrogen bonds and other non-covalent interactions within the mixtures, providing a robust framework for understanding the molecular behavior of these systems.

FT-IR Analysis

To understand the presence of intermolecular interactions and H-bonding, the FT-IR spectra of pure components and their binary mixtures at three different composition ratio such as 4:1, 1:1 and 1:4 were recorded at 298.15K.

On basis of secondary properties and computational calculation results, the test is focused on five functional groups' frequencies which contributes their major role in overall interactions such as intermolecular H-bonding (v_{O---H}), free phenolic $-OH$ stretching (v_{O-H}), aliphatic $C-H$ symmetrical stretching (v_{C-H}), aromatic $C-H$ symmetrical stretching (v_{C-H}) and$C-X$(X=halogen atoms) symmetrical stretching (v_{C-X}) of halobenzene.

The experimentally obtained frequencies values of pure components and their binary mixtures as well as the values of theoretically calculated frequencies using B3LYP/6-31+G(d,p) method with their shift values with comparison respect to α-terpineol and halobenzene are listed in Table S15 of supplementary data. The spectra of pure components and binary mixtures at different composition ratios are as shown in Fig. 16, Fig. 17 and Fig. 18 and Figs. S19 to S28 of supplementary data file.

The standard characteristics IR frequencies for selected functional groups are 3200-3600 cm^{-1} for hydrogen bonding (v_{O---H}), 3500-3700 cm^{-1} free phenolic $-OH$ stretching (v_{O-H}), 3000-2850 cm^{-1} for aliphatic $C-H$ symmetrical stretching (v_{C-H}), 3000-3100 cm^{-1} for aromatic $C-H$ symmetrical stretching (v_{C-H}) and $C-X$ stretching (v_{C-X}) (1000-1250 cm^{-1} for $C-F$, 1089-1096 cm^{-1} for $C-Cl$and 1000-1080 cm^{-1} for $C-Br$ stretching[56,57].

As our earlier discussion of computational analysis, the oxygen atom is involved in H-bonding formation with H-atoms attached with aromatic ring's carbons of halobenzenes. Here, values of shift of free phenolic $-OH$ group frequency (v_{O-H}) with respect to pure α-terpineol values are positive for fluorobenzene binary mixtures and these values shift toward the negative values with changing of fluorobenzene to bromobenzene component in binary mixture. These

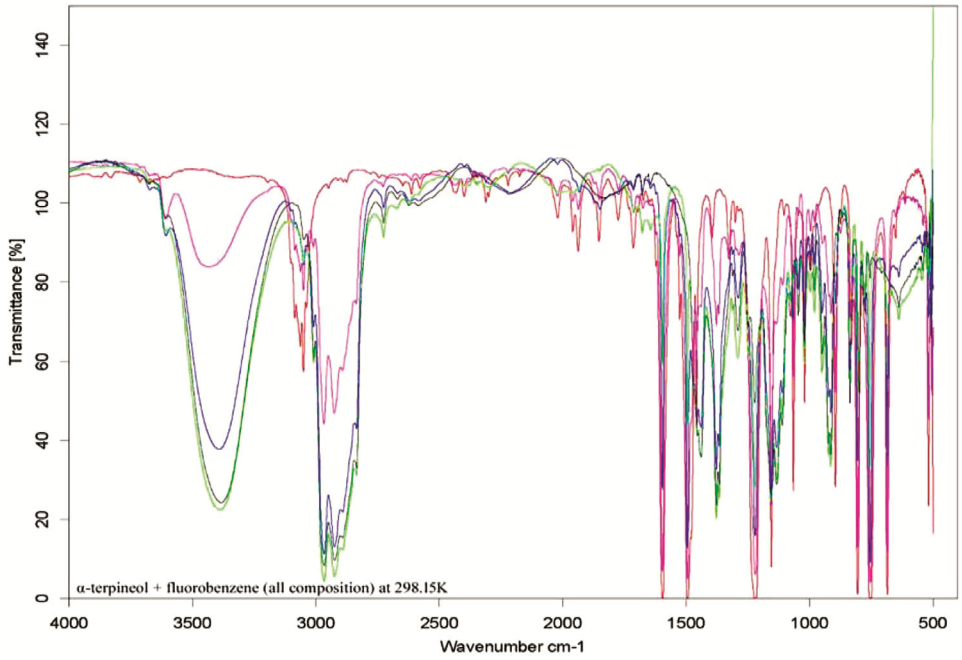

Fig. 16 — Experimental FT-IR transmittances spectra at 298.15K for α-terpineol (1) + Fluorobenzene (2); ——, pure fluorobenzene; ——, 4:1 composition ratio; ——, 1:1 composition ratio; ——, 1:4 composition ratio and ——, pure α-terpineol.

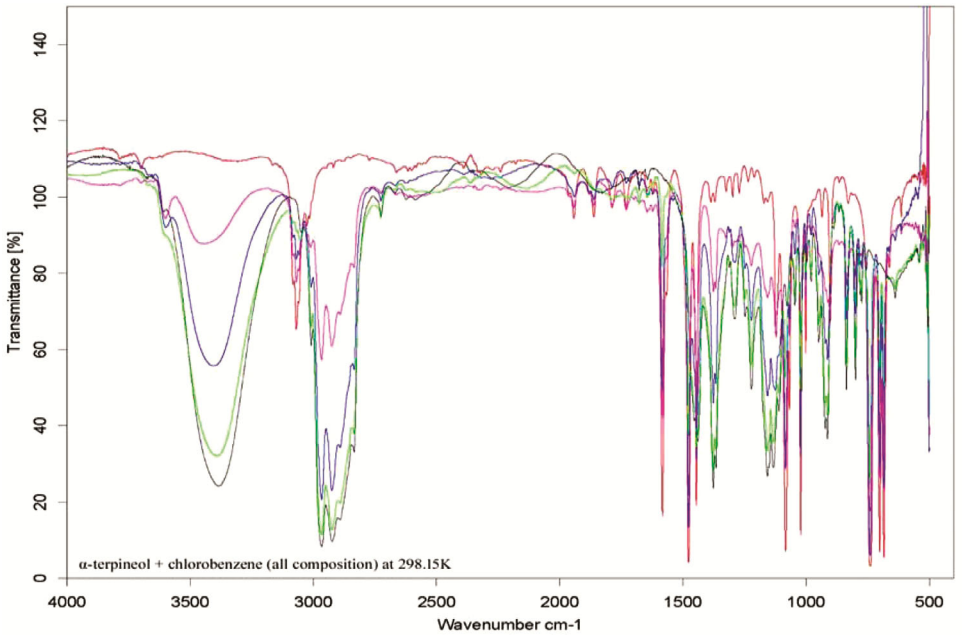

Fig. 17 — Experimental FT-IR transmittances spectra at 298.15K for α-terpineol (1) + Chlorobenzene (2); ——, pure chlorobenzene; ——, 4:1 composition ratio; ——, 1:1 composition ratio; ——, 1:4 composition ratio and ——, pure α-terpineol.

facts indicate that the fluoro atom of fluorobenzene act as a stronger proton acceptor (electron density donor) than chloro and bromo atom. Due to this phenomenon, the excess electron density added to $-OH$ group. So, the required energy for stretching of $O-H$ functional group becomes higher than it is in pure component state. So, it shows the positive shift in $-OH$ frequency in α-terpineol + fluorobenzene binary mixtures. It also indicates that fluoro atom is strongly attached with α-terpineol molecules in comparison of chlorobenzene and bromobenzene molecules.

Similarly, the hydrogen atoms of aliphatic $-CH_3$ groups also involved in intermolecular interactions with halobenzene molecules and this fact is supported by

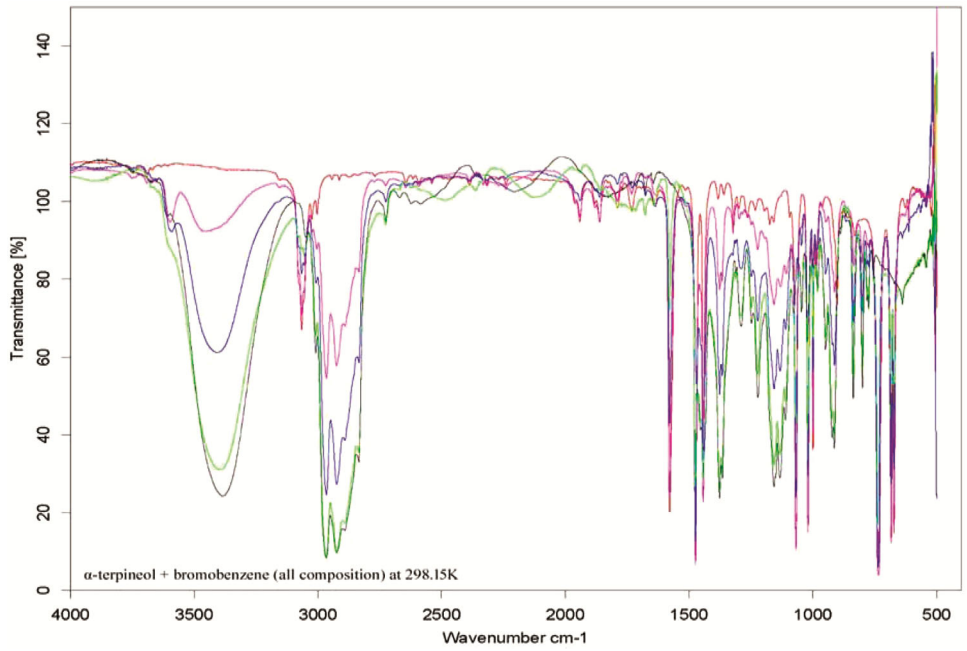

Fig. 18 — Experimental FT-IR transmittances spectra at 298.15K for α-terpineol (1) + Bromobenzene (2);———, pure bromobenzene; ———, 4:1 composition ratio; ———, 1:1 composition ratio; ———, 1:4 composition ratio and ———, pure α-terpineol.

the positive shift value of aliphatic $C-H$ functional group frequency (υ_{C-H}) in comparison of α-terpineol values of aliphatic $C-H$ functional group frequency (υ_{C-H}) in pure component.The shift values of (υ_{O---H}) (H-bonding) indicates that the H-bonding becomes stronger at higher concentration of halobenzene.

So, the results obtained from FT-IR analysis indicate the presence of H-bonding and delocalization type intermolecular interaction between components of binary mixtures and supports the results obtained from other methods.

Conclusion

The comprehensive analysis of physical properties such as V_m^E, $\bar{V}_{m,1}^{o,E}$, $\bar{V}_{m,2}^{o,E}$, Δk_s, $\bar{K}_{s,m,1}^{o,E}$, $\bar{K}_{s,m,2}^{o,E}$,$V_{m,\Phi,1}^{o}$, E_Φ^o, Δu and Δz, highlights the presence of strong intermolecular interactions within the binary mixtures studied. The observed negative values of V_m^E, $\bar{V}_{m,1}^{o,E}$, and Δk_salong with the positive values of $V_{m,\Phi,1}^{o}$, E_Φ^o,Δu, and Δz, suggest significant hydrogen bonding and delocalization-type interactions between the components.

The derived empirical parameters from the Redlich-Rosenberg-Mayer equation further corroborate the presence of these interactions, confirming the strong intermolecular associations within the mixtures. Notably, the variation of excess property values with temperature implies a reduction in interaction strength at elevated temperatures, estimating the temperature sensitivity of these intermolecular forces and their influence on the stability and behavior of the mixtures.

Additional support for these findings comes from FT-IR spectral and computational analyses, which provide evidence for the formation of new hydrogen bonds and delocalization interactions. Specifically, the shifts in the frequencies of functional groups, such as –OH, indicate the formation of strong hydrogen bonds. Computational analyses, particularly the second-order perturbation energies from NBO analysis, reveal the most robust intermolecular associations between the oxygen lone pairs of α-terpineol and the hydrogen atoms of halobenzenes (fluorobenzene) at both possible interaction sites.

Overall, the data strongly suggest that α-terpineol exhibits significant intermolecular interactions with halobenzenes, primarily driven by the –OH groups' ability to engage in hydrogen bonding and delocalization interactions with charged atoms in the binary mixtures. The presence of fluorine in halobenzenes further enhances these electrostatic interactions, solidifying the findings of strong intermolecular associations. Based on the various observations taken from various analytical and computational tools, the order of interaction strength between halobenzene and α-terpineol is summarized as: Fluorobenzene>Chlorobenzene>Bromobenzene.

Acknowledgement

The authors are thankful to the Department of Chemistry, Hemchandracharya North Gujarat University, Patan, Gujarat, India for providing the necessary facilities to carry out the work.

Supplementary Information

Supplementary information is available in the website http://nopr.niscpr.res.in/handle/123456789/58776.

References

1 Khaleel C, Tabanca N & Buchbauer G, *Open Chem*, 16 (2018) 349.
2 Bakkali F, Averbeck S, Averbeck D & Idaomar M, *Food Chem Toxicol*, 46 (2008) 446.
3 Iahtisham-Ul-Haq, Khan S, Sohail M, Iqbal M J, Awan K A & Nayik G A, *In Essential Oils* (Academic Press), 2023, p. 479.
4 Hunter M, *Essential oils art, agriculture, science, industry and entrepreneurship (a focus on the Asia-Pacific region)* (Nova Science Publishers, Inc, New York), 2009.
5 Buchbauer G & Baser K H C, *Handbook of Essential oils: Science, Technology, and Applications* (CRC Press), 2023.
6 Burdock G A, *Fenaroli's Handbook of Flavor Ingredients Fenaroli's Handbook of Flavor Ingredients*, 6th Edn (CRC Press), 2010.
7 Saravanakumar K, Lavanya T G, Baskaran R & Kubendran T R, *J Iran Chem Soc*, 9 (2012) 277.
8 Patel P & Sharma S, *Indian J Chem*, 62 (2023) 575.
9 Ceulemans J, *In Intermolecular Forces: An Introduction to Modern Methods and Results*, (Springer Berlin Heidelberg), 2023, p. 459.
10 Boumahraz M, Davydov V Y, Gonzalez M E & Kiselev A V, *Chromatographia*, 17 (1983) 143.
11 Patel P & Sharma S, *Indian J Chem*, 59A (2020) 797.
12 Riddick J A, Bunger W B & Sakano T K, *Organic solvents: physical properties and methods of purification*, 4th Edn, (John Wiley and Sons, New York), 1986.
13 Furniss B S, *Vogel's textbook of practical organic chemistry* (Pearson Education, India), 2011.
14 Hohenberg P, *Phys Rev*, 136 (1964) B864.
15 Kohn W & Sham L J, *Phys Rev*, 140 (1965) A1133.
16 Parr R G & Yang W, *Density-functional theory of atoms and molecules* (Oxford University Press, New York & Clarendon Press, Oxford), 1989.
17 Salahub D R & Zerner M C, *The Challenge of d and f Electrons: Theory and Computation* (ACS Publications), 1989.
18 Labanowski J K & Andzelm J W, *Density functional methods in chemistry* (Springer Science & Business Media), 2012.
19 Andzelm J & Wimmer E, *J Chem Phys*, 96 (1992) 1280.
20 Becke A D, *J Chem Phys*, 96 (1992) 2155.
21 Gill P M W, Johnson B G, Pople J A & Frisch M J, *Chem Phys Lett*, 197 (1992) 499.
22 Stratmann R E, Burant J C, Scuseria G E & Frisch M J, *J Chem Phys*, 106 (1997) 10175.
23 Carpenter J E, *Extension of Lewis structure concepts to open-shell and excited-state molecular species* (University of Wisconsin, Madison), 1987.
24 Carpenter J E & Weinhold F, *J Mol Struct Theochem*, 169 (1988) 41.
25 Foster J P & Weinhold F, *J Am Chem Soc*, 102 (1980) 7211.
26 Reed A E & Weinhold F, *J Chem Phys*, 78 (1983) 4066.
27 Reed A E, Weinstock R B & Weinhold F, *J Chem Phys*, 83 (1985) 735.
28 Reed A E & Weinhold F, *J Chem Phys*, 83 (1985) 1736.
29 Reed A E, Curtiss L A & Weinhold F, *Chem Rev*, 88 (1988) 899.
30 Naaman R & Vager Z, *The structure of small molecules and ions* (Springer Science & Business Media), 2012.
31 Frisch M J, Trucks G W & Schlegal H B, Gaussian 16, Revision A.03, Gaussian Inc, Wallingford CT, 2016.
32 Dennington R, Keith T A & Millam J M, Gauss View 06, 2016.
33 Lu T & Chen F, *J Comp Chem*, 33 (2012) 580.
34 Humphrey W, Dalke A & Schulten K, *J Mol Graph*, 14 (1996) 33.
35 Nain A K, *J Chem Thermodyn*, 60 (2013) 105.
36 Bahadur I & Deenadayalu N, *Thermochim Acta*, 566 (2013) 77.
37 Singh S, Parveen S, Shukla D, Yasmin M, Gupta M & Shukla J P, *J Sol Chem*, 40 (2011) 889.
38 Junjie Z, *J China Univ Sci Tech*, 14 (1984) 298.
39 Nomoto O, *J Phys Soc Japan*, 13 (1958) 1528.
40 Van Dael W & Vangeel E, *Proceedings of the First International Conference on Calorimetry and Thermodynamics:* Warszawa, (PWN-Polish Scientific Publishers), 1969.
41 Jacobson B, *J Chem Phys*, 20 (1952) 927.
42 Bhalodia J & Sharma S, *J Solution Chem*, 42 (2013) 1794.
43 Redlich O & Kister A T, *Ind Eng Chem*, 40 (1948) 341.
44 Kondaiah M, Sreekanth K, Kumar D S, Nayeem S M & Rao D K, *J Therm Anal Calorim*, 118 (2014) 475.
45 Saravanakumar K & Kubendran T R, *Res J Chem Sci*, 2 (2012) 50.
46 Bhuiyan M M H & Uddin M H, *J Mol Liq*, 138 (2008) 139.
47 Keshapolla D & Gardas R L, *Fluid Phase Equilib*, 383 (2014) 32.
48 Patel P, Bhalodia J, Sharma S S & Jha P C, *J Mol Liq*, 222 (2016) 1192.
49 Sharma T, Rani R, Kumar A & Bamezai R K, *J Solution Chem*, 48 (2019) 658.
50 Das D, Das B & Hazra D K, *J Mol Liq*, 115 (2004) 135.
51 Das D, Das B & Hazra D K, *J Mol Liq*, 111 (2004) 15.
52 Hammami F, Issaoui N & Nasr S, *Comp Theor Chem*, 1199 (2021) 113218.
53 Otero-De-La-Roza A, Johnson E R & Contreras-García J, *Phys Chem Chem Phys*, 14 (2012) 12165.
54 Toro-Labbé A, *Theoretical Aspects of Chemical Reactivity*, (Elsevier Publisher), 2007.
55 Schmider H L & Becke A D, *J Mol Struct Theochem*, 527 (2000) 51.
56 Silverstein R M, Bassler G C & Morrill T C, *Spectrometric Identification of Organic Compounds,* (Wiley Publisher), 1981.
57 National Bureau of Standards - U.S. Government Printing Office, NSRDS-NBS: National Standard Reference Data Series. Retrieved from https://nvlpubs.nist.gov/nistpubs/Legacy/NSRDS/nbsnsrds6.pdf.